

Thalamic deep brain stimulation in traumatic brain injury: a phase 1, randomized feasibility study

Received: 11 August 2023

Accepted: 10 October 2023

Published online: 04 December 2023

 Check for updates

Nicholas D. Schiff^{1,2}✉, Joseph T. Giacino^{3,4}, Christopher R. Butson^{5,6}, Eun Young Choi⁷, Jonathan L. Baker¹, Kyle P. O'Sullivan⁵, Andrew P. Janson^{5,8}, Michael Bergin³, Helen M. Bronte-Stewart⁷, Jason Chua⁹, Laurel DeGeorge¹, Sureyya Dikmen¹⁰, Adam Fogarty⁷, Linda M. Gerber^{9,11}, Mark Krel⁷, Jose Maldonado¹², Matthew Radovan¹³, Sudhin A. Shah¹⁴, Jason Su¹⁵, Nancy Temkin¹⁶, Thomas Tourdias¹⁷, Jonathan D. Victor^{1,2}, Abigail Waters³, Stephanie A. Kolakowsky-Hayner⁷, Joseph J. Fins¹¹, Andre G. Machado¹⁸, Brian K. Rutt^{19,20,21} & Jaimie M. Henderson^{7,20,21}✉

Converging evidence indicates that impairments in executive function and information-processing speed limit quality of life and social reentry after moderate-to-severe traumatic brain injury (msTBI). These deficits reflect dysfunction of frontostriatal networks for which the central lateral (CL) nucleus of the thalamus is a critical node. The primary objective of this feasibility study was to test the safety and efficacy of deep brain stimulation within the CL and the associated medial dorsal tegmental (CL/DTTm) tract. Six participants with msTBI, who were between 3 and 18 years post-injury, underwent surgery with electrode placement guided by imaging and subject-specific biophysical modeling to predict activation of the CL/DTTm tract. The primary efficacy measure was improvement in executive control indexed by processing speed on part B of the trail-making test. All six participants were safely implanted. Five participants completed the study and one was withdrawn for protocol non-compliance. Processing speed on part B of the trail-making test improved 15% to 52% from baseline, exceeding the 10% benchmark for improvement in all five cases. CL/DTTm deep brain stimulation can be safely applied and may improve executive control in patients with msTBI who are in the chronic phase of recovery. ClinicalTrials.gov identifier: [NCT02881151](https://clinicaltrials.gov/ct2/show/study/NCT02881151).

msTBI often leads to enduring physical, cognitive, emotional and behavioral impairments^{1–7}. Cognitive dysfunction is the dominant factor underlying persistent functional disability following msTBI^{5,6,8} and correlates with both injury severity and performance on standardized neuropsychological assessments⁹. Characteristically, cognitive dysfunction in msTBI impacts executive control underlying task-switching

and organizing activities, sustained attention, information-processing speed and resistance to mental fatigue^{5–8,10}. The msTBI population is estimated to number more than 5 million individuals in the United States¹¹ who remain unable to return to previous levels of functioning within their communities¹². At present, there is no effective therapy for the disabling effects of injury-related impairments in attention,

executive function, working memory or information-processing speed. The sustained nature of cognitive impairment in msTBI contrasts with the more transient impairments seen in mild TBI¹³, suggesting that the underlying pathophysiologic mechanisms of msTBI and mild TBI are distinct. The specific pathophysiology of msTBI suggests both a mechanism and a potential remediation strategy and these considerations motivated this study.

Several lines of evidence indicate that the major persistent cognitive deficits in msTBI primarily reflect dysfunction of neurons within the frontal cortex and striatum^{5,6,10,14–16}, including a set of medial prefrontal regions (particularly rostral anterior cingulate cortex, medial prefrontal and supplementary motor area) with strong functional interconnectivity. Cognitive impairment following msTBI is further linked with alteration of subcortical functional and structural connections of these frontal cortical regions with subcortical structures^{15,17,18}. Atrophy of the left thalamus has been specifically correlated with executive dysfunction after msTBI¹⁸.

A critical brain region linking these frontal cortical and striatal neurons into ‘frontostriatal’ networks supporting executive functions is the CL nucleus of the thalamus^{19–25}. CL neurons provide input to prefrontal/frontal cortex and striatum^{19–25} and optogenetic stimulation of CL activates these structures extensively in rodents²⁵. Individual CL neurons broadly innervate the rostral striatum and frontal cortex²¹. CL projections to specific layers of the cortex support its unique role in enhancing activity of its cortical target regions^{20,23}. Within the striatum, CL projections are particularly effective in driving action potentials from primary striatal output neurons²², which in turn increases their inhibition of the globus pallidus pars interna, further releasing additional thalamic activation of the cortex (Extended Data Fig. 1). Collectively, these specializations likely enable recruitment of CL neurons by forebrain arousal regulation mechanisms during effortful mental activities which tax sustained attention, planning, decision-making and working-memory resources^{19,20,26}. Underactivation of CL is proposed as a key factor in functional downregulation of frontostriatal networks after brain injuries under the ‘mesocircuit hypothesis’²⁷ for functional recovery from impaired consciousness; incomplete recovery of neuronal function within these same networks is proposed to underlie persistent cognitive slowing and impaired executive function²⁷. These observations suggest a practical therapeutic strategy for reversing the enduring cognitive deficits in msTBI: direct electrical stimulation of the remaining functional afferents emanating from CL via deep brain stimulation (DBS) (Extended Data Fig. 1).

We sought to translate these insights into a practical strategy for human CL DBS by performing a feasibility study (NCT02881151) to evaluate its safety and efficacy in human participants with chronic TBI-related disability impacting everyday function and employability. Informed by our previous studies in humans²⁸ and nonhuman primates^{19,29}, we chose the lateral portion (‘wing’) of the CL thalamic nucleus along with its associated fiber bundle, the DTTm^{19,29,30}, as the stimulation target (Supplementary Fig. 1a–f). We developed biophysical models to guide virtual DBS electrodes within each individual’s CL/DTTm to stimulate along the axis of the CL/DTTm fiber bundle based on location and stimulation amplitudes³¹ and used the predicted activation models to evaluate and set criteria for successful CL/DTTm activation. The use of new imaging and thalamic segmentation protocols, as well as predictive biophysical models estimating activation of projection fibers, enabled very precise and accurate location of the CL nucleus and DTTm fiber bundle in individual human participants. We then examined the safety and efficacy of this intervention for improving the persistent cognitive deficits of msTBI. As the primary efficacy end point, we selected part B of the trail-making test (TMT-B), based on the well-established relationship between the diffuse axonal injury produced by msTBI and persistent dysfunction in attentional control and information-processing speed^{5,6,8,9,32}.

Results

Patient disposition

Based on patient recruitment activities (Supplementary Information), we received 419 inquiries for information about the trial. Candidates initially underwent telephone screening, which included administration of the Glasgow Outcome Scale-Extended (GOS-E) structured interview to ensure that the candidate had not returned to pre-injury levels of vocational or educational function. From these initial inquiries, 15 individuals were consented for further assessment to confirm eligibility. Consent was obtained under a single Institutional Review Board (IRB)-approved protocol at Stanford University. Of these, nine candidates were excluded and six met all eligibility criteria and were enrolled and randomized between August 2018 and May 2021 (Fig. 1). The six adults enrolled all had a history of moderate-to-severe TBI (Glasgow Coma Scale (GCS) score, 3–12) with persistent neuropsychological impairment and functional disability (GOS-E score, 5–7)³³ (Methods). We established baseline cognitive, psychological and quality-of-life status (Table 1). We sought to recruit participants who were representative of the general population of those with msTBI in terms of sex, which is anticipated to yield a 2:1 male:female ratio; ultimately, we enrolled four men and two women based on self-report. We did not collect disaggregated sex and gender information.

Following CL/DTTm DBS implantation, participants were randomly assigned to one of three postsurgical baseline conditions lasting 30, 44 or 58 d. The staggered baseline design was intended to identify acute CL/DTTm DBS effects within individual participants and across participant pairs in response to initial stimulation exposure (short, intermediate or long baseline). Participants next entered a 14-d stimulation titration phase to identify optimal stimulation parameters. After completion of the titration phase, participants completed a 90-d open-label treatment phase during which they were exposed to CL/DTTm DBS for 12 h per day. Finally, participants were randomly assigned to a 21-d treatment withdrawal or continuation condition to assess for loss of effect; this was double-blinded to minimize the influence of examiner and participant bias on final outcome assessment. The outcome assessment battery and electrophysiological studies (described below) were repeated upon completion of the postsurgical washout, treatment and post-treatment withdrawal phases. The primary end point was the change in completion time on the TMT-B from presurgical baseline to the end of the 90-d treatment phase (Supplementary Information provides a discussion of study design considerations).

Primary end points

TMT-B served as the primary outcome measure. Performance on the TMT-B is thought to reflect executive control of attention, as working memory and set-switching capacity are challenged under speeded conditions³⁴. We defined our primary end point as at least a 10% decrease (improvement) in completion time from presurgical baseline to the end of the treatment phase. Similarly, we defined decline as at least a 10% increase (worsening) in TMT-B completion time from presurgical baseline to the end of the treatment phase (Methods).

Five of the six participants completed all four outcome assessments (the sixth participant exited the study before the titration phase). All participants met the preselected primary end point (benchmark, 10% improvement from presurgical baseline to the end of the treatment phase; average improvement 31.75%; range 15–52%) (Fig. 2a). While the two participants with the greatest initial deficits (P3 and P6; Extended Data Table 1) experienced the most improvement (>40%), even those whose baseline performance was within the normal range (P4 and P5) improved by more than 20% (Extended Data Table 1). For the demographically adjusted T-scores (mean = 50, s.d. = 10), the average improvement was 9.6 points (Extended Data Table 1), which represents a change of approximately one s.d. of the population distribution³⁵.

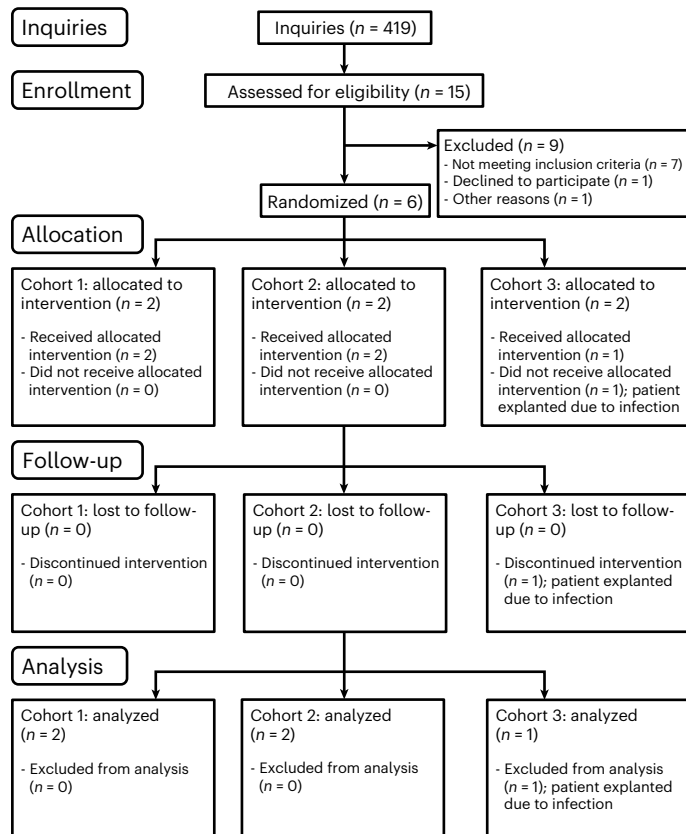


Fig. 1 | CONSORT diagram. The study CONSORT diagram. CONSORT, Consolidated Standards of Reporting Trials.

Secondary end points

On the prespecified secondary end point, change in TBIQoL-Fatigue, two participants met the improvement benchmark, two remained stable and one met the benchmark for decline (Fig. 2c). On the TBIQoL-Executive Function subscale, four of the five participants who completed the trial exceeded the 10% improvement benchmark (mean = 32.7%, min = 0, max = 62%).

Figure 2c shows the number of participants who exceeded the 10% improvement benchmark on each measure in the test battery. All five study participants also showed improved performance on the TMT-A, which assesses visual search speed³⁴ and may be linked to frontostriatal function and information-processing speed (as discussed below). All five participants also met the 10% improvement benchmark for the TBIQoL-Attention subscale (mean = 79.5%, min = 50, max = 130%).

The Ruff 2&7 test, a measure of selective attention under speeded conditions, also showed broad improvements (Fig. 2c, Supplementary Table 2 and Supplementary Methods) across the four participants who completed this test in full (P1's data were invalidated due to test administration error). All four participants showed improved speed difference greater than 10% (range 12% to 68% improvement in 'Total Speed'; Supplementary Table 1) and three of the four showed improvements in controlled search speed (17% to 70% improvement; Supplementary Table 1) and auto detection speed (20% to 54% improvement; Supplementary Table 1; additional behavioral results are shown in Supplementary Tables 2–6).

Two participants (P1 and P4) improved in global level of functioning from the lower moderate disability category of the GOS-E to the upper-moderate disability category. These changes reflect recovery of work capacity (from inability to work to work at reduced capacity) and resumption of routine social activities with family and friends. Functional status remained stable in the other three participants

(P3, lower moderate disability; P5 and P6, upper moderate disability; Supplementary Tables 2–6).

As part of the study plan, TMT-B performance was also measured at two intermediate time points (postsurgical and treatment start), both of which followed some exposure to DBS. As measurements at these time points likely were influenced by a wide range of other factors (for example the surgery itself, time from surgery and hours of stimulation exposure before measurement), they were not part of the prespecified outcome assessment. For completeness, these results are shown in Extended Data Fig. 2. Three of five participants agreed to participate in a planned randomized blinded withdrawal phase (Supplementary Information and Supplementary Table 7). Only one participant randomized to the OFF (DBS amplitudes set to zero) condition (P3) and demonstrated a 34% decline in TMT-B score consistent with a withdrawal effect.

In addition, each participant and family members underwent semi-structured interviews as part of a parallel study (Supplementary Table 8)^{36,37}.

Safety

Safe conduct of the study was monitored by a clinical oversight committee consisting of the five Principal Investigators (PIs) (J.M.H., N.D.S., J.T.G., C.R.B. and A.G.M.) and two independent medical monitors. The committee was convened at the beginning of the study and met quarterly to discuss study progress. All adverse events were reviewed with the committee and their adjudication agreed on following group discussion. Study continuation was predicated on a unanimous vote of the committee at each meeting.

All six participants underwent successful placement of bilateral DBS leads (Medtronic 3387) with no acute complications. There were 14 adverse events, 2 of which were classified as serious (requiring hospitalization) (Supplementary Table 9). All adverse events resolved without sequelae. The majority of adverse events were mild and self-limiting, consisting of typical postoperative symptoms. One participant developed a postoperative scalp infection requiring explantation of the system before the titration phase of the study. This participant was subsequently withdrawn from the study. One participant experienced back pain, neck pain, headache and hamstring tightness beginning several days after surgery, which were attributed to possible aseptic meningitis. These symptoms resolved over the course of 1 week. Another participant experienced difficulty with planning, organization and word recall, which persisted over the course of approximately 2 months and was felt to be possibly due to stimulation.

Post-hoc analyses

Inter-subject consistency of electrode implantations within the human CL/DTTm. To translate preclinical findings that identified CL neurons²⁵, the 'lateral wing'^{19,25} and the associated DTTm fiber bundle^{19,29,30} as the primary structure for DBS activation, we developed a specialized data processing pipeline (Supplementary Information and Supplementary Fig. 1a–f). Figure 3a–f illustrates the approach to post-implant target localization and stimulation in a representative participant (P5). Figure 3a,d identifies the location of active electrode contacts (L3 and L4 on the left side, R3 and R4 on the right side) displayed on coronal white-matter-nulled (WMn) images with CL boundaries shown in red. Figure 3c,f shows CL/DTTm fiber bundle model activation achieved within the left and right hemispheres. Relative activation was estimated by calculating the percentage of fibers in each fiber tract that reached the threshold for activation³¹; these percentages were expressed using a histogram for each of four key fiber tracts for each lead position: CL/DTTm, mediodorsal (MD), ventral posterolateral (VPL) and centromedian (Cm) (Fig. 3b,d for left and right sides, respectively). In this participant, combined stimulation of the four active contacts achieved a predicted 81% activation of CL/DTTm fibers within the left hemisphere and 78% activation of these

Table 1 | Patient demographics table

Participant	1	2	3	4	5	6	Mean
Demographics							
Age (years)	39	38	60	22	30	28	36.2
Years since injury	18	2	3	4	10	9	7.7
Years education	16	14	13	13	14	14	14
Sex	F	F	M	M	M	M	
Injury characteristics							
Previous TBI	N	N	Y	N	N	N	
Cause of injury	MVA	MVA	Fall ^a	MVA ^b	MVA	Fall ^c	
Highest level of care	ICU	ER	ICU	ICU	ICU	ICU	
Loss of consciousness	Y	Y	Y	Y	Y	Y	
GOS-E pre-surgery	5	5	5	5	6	6	
Return to previous employment/academic level (yes/no)	No	No	No	No	No	No	
Self-reported symptoms (+ present/- absent)							
Cognitive-behavioral							
Hypoarousal/lethargy/somnolence	-	-	-	+	+	-	
Fatigue	+	+	+	+	+	-	
Insomnia/sleep disturbance	-	+	-	+	+	-	
Confusion	-	+	+	+	-	-	
Thinking abnormality	-	-	-	-	-	+	
Attention impairment	+	-	+	+	+	-	
Memory impairment/amnesia	+	+	+	+	+	+	
Language impairment	+	-	-	+	+	-	
Slurred speech	-	+	-	+	-	-	
Executive function impairment	+	+	-	+	+	-	
Motor restlessness/hyperkinesia	+	+	-	+	-	-	
Agitation/aggression	+	+	-	-	+	-	
Irritability	+	+	-	+	+	-	
Nervousness	+	+	-	-	+	-	
Depression	+	+	+	-	+	-	
Anxiety	+	+	+	-	+	-	
Paranoid reaction	-	-	-	-	+	-	
Sensory-motor							
Decreased visual acuity	-	+	+	-	+	-	
Sensitivity to light	-	+	+	-	+	-	
Dizziness/lightheadedness	-	+	-	+	+	-	
Weakness	-	-	-	-	+	-	
Involuntary muscle contractions	+	-	-	-	-	-	
Pain							
Headaches	+	+	+	+	+	-	
Limb pain	-	-	-	-	+	-	
Abdominal pain	-	-	-	-	+	-	
Chest pain	-	-	-	-	+	-	
General medical							
Nausea	-	-	-	-	+	-	
Constipation	-	-	-	-	+	-	
Diarrhea	-	-	-	-	+	-	
Dysphagia	+	-	-	-	-	-	
Urinary retention	-	-	-	-	+	-	

Table 1 (continued) | Patient demographics table

Participant	1	2	3	4	5	6	Mean
Hypertension	-	-	-	-	+	-	
Skin rash	-	-	-	-	-	+	
Pruritis	+	-	-	-	-	+	
Hair loss	-	-	-	-	+	-	
Presurgical test performance (executive measures)							
TMT completion time (s)							
Part A	62	38.7	85.9	22.1	18.7	61.6	48.2
Part B	153.0	80.8	171.7	39.0	42.6	166.6	109.0
TMT, demographically adjusted T-scores							
Part A	21	32	20	49	57	22	33.5
Part B	22	38	33	62	62	22	39.8
TBIQoL Att/Concent v.1 SF6a total raw score	19	12	6	14	10	14	12.5
TBIQoL Exec Func v.1 SF10a total raw score	36	23	20	25	28	24	26.0

Table describes patient demographics. MVA, motor vehicle accident. GOS-E, range 1 (dead) to 8 (return to normal life); TMT, range 0–300s. TBIQoL Att/Concent v.1 SF6a, Traumatic Brain Injury – Quality of Life Attention and Concentration v.1.0 6-item Short Form (range 6–30, higher scores indicate greater symptom burden); TBIQoL Exec Func v.1 SF6a, Traumatic Brain Injury – Quality of Life Executive Function v.1.0 ten-item Short Form (range 10–50, higher scores indicate better performance). *Fall from 450 feet. †Bicyclist hit by motor vehicle. ‡Fall from five stories.

fibers within the right hemisphere. The histograms plotted in Fig. 3b,e show the percentage of activation for CL/DTTm, MD, VPL and Cm fibers with voltages between 1 V and 5 V applied to each of the four contacts. For most contacts, CL/DTTm fiber activation dominated the range of current (or voltage; Methods) amplitudes modeled for single contact monopolar activation. These histograms guided interpretations of findings obtained during titration testing used to establish selection of specific electrode contacts and stimulation parameters in the treatment trial (Methods and Extended Data Figs. 3–7).

Based on the activation profiles modeled for each participant (Fig. 3 and Extended Data Figs. 3–7), we sought electrode positions and orientations that were predicted to provide strong and selective activation of the target CL/DTTm fibers, compared to fibers associated with MD, VPL and Cm. The activation profiles predicted for the combination of active electrode contacts chosen for each participant by hemisphere are shown in Fig. 3g. In all participants, selective and strong activation of left-hemisphere CL/DTTm fibers was predicted, though the degree of selectivity varied. Predicted activation of right-hemisphere CL/DTTm showed greater variability. In P4, our presurgical modeling did not predict activation of modeled right-hemisphere CL/DTTm fibers from the postoperative placement of this electrode (0.5% predicted activation) but as shown below electrophysiological measurements demonstrate similar activation patterns of both hemispheres in P4; this discrepancy was hypothesized to reflect distortion effects of a small hemorrhage within the right thalamus on the diffusion tensor imaging (DTI) modeling, leading to a drop out of modeled fibers (Extended Data Figs. 5 and 6 and Discussion). Final stimulation parameters for each participant were chosen after a sequence of titration testing steps during which stimulation parameters adjusting the shape of the activation field (contact geometries, amplitudes of current or voltage, and pulse width of stimulation) were adjusted to maximize activation of modeled CL/DTTm, limit activation of modeled avoidance fibers and strictly eliminate observed side effects during testing (Supplementary Information, titration phase). Across the participants final parameters ranged: 150–185 Hz, 60–90 μ s pulse width, 3.1–4.0 V/3 mA, 3.3–5.1 μ C cm^{-2} per phase.

To compare electrode placements across the five participants, we developed a synthetic atlas to organize all participant electrode placements within a single common brain space (Methods). Figure 4a–c illustrates the placements of active contacts for all participants in this common synthetic atlas space, demonstrating a tight clustering of

active contacts for left-hemisphere electrodes around the emergence of the CL/DTTm fibers exiting the CL nucleus boundary, with greater spatial variability for the active right-hemisphere electrode contacts, particularly the lower active contact. This reduced placement precision on the right side was felt to be due to brain shifts induced by loss of cerebrospinal fluid during the procedures as the right hemisphere electrodes were placed after the left in four of five participants that completed the trial. Supplementary Videos 1 and 2 (left to right, showing preoperative versus postoperative contacts, respectively) compare the presurgical and postsurgical placement clusters illustrating that left hemisphere postsurgical placements adhered closely to the initial plan with larger discrepancies between pre- versus post-placements on the right side. Supplementary Video 3 illustrates the surgical planning and outcome assessment process. Fig. 3g graphs the relative activation percentage for CL/DTTm and the avoidance fibers from MD, VPL and Cm. For all participants, left-hemisphere electrodes produced strong activation of the modeled CL/DTTm fibers; right hemisphere lower contacts showed greater variability.

To establish and evaluate consistency of physiological effects across participants, we measured evoked responses in the electroencephalogram (EEG) to repetitive low-frequency stimulation (Methods). Figure 5 shows superimposed cortical evoked potential time tracings obtained across a 256-channel EEG array for activation across two therapeutic contacts (obtained before treatment phase, excepting P3; Supplementary Table 11). Evoked potentials were driven by 100-ms trains of stimulation (150–185 Hz) on a 2-Hz duty cycle of stimulation (Supplementary Table 12 shows full stimulation parameters for each participant); stimulation bouts occur at 0–100 ms on the displayed plots (gray shade; Fig. 5a,c, Methods and Supplementary Figs. 2–11). Across both hemispheres, evoked responses typically demonstrated an initial positive deflection peaking at \sim 200 ms (vertical red lines; Fig. 5). Topographical plots indicating the spatial variation in depth of evoked response at the time of the peak (\sim 200 ms) show that the strongest response appears within the frontal regions of the ipsilateral hemisphere between the medial and lateral regions (Supplementary Figs. 2–11 provide channel-by-channel evoked response profiles). As seen in Fig. 5, the left hemisphere showed more reproducible localization, depth of modulation and timing of peaked amplitude responses across all participants. Comparing these findings to those obtained from the synthetic atlas in Fig. 4, this likely corresponds to the tighter clustering of the left versus right electrode contact placements

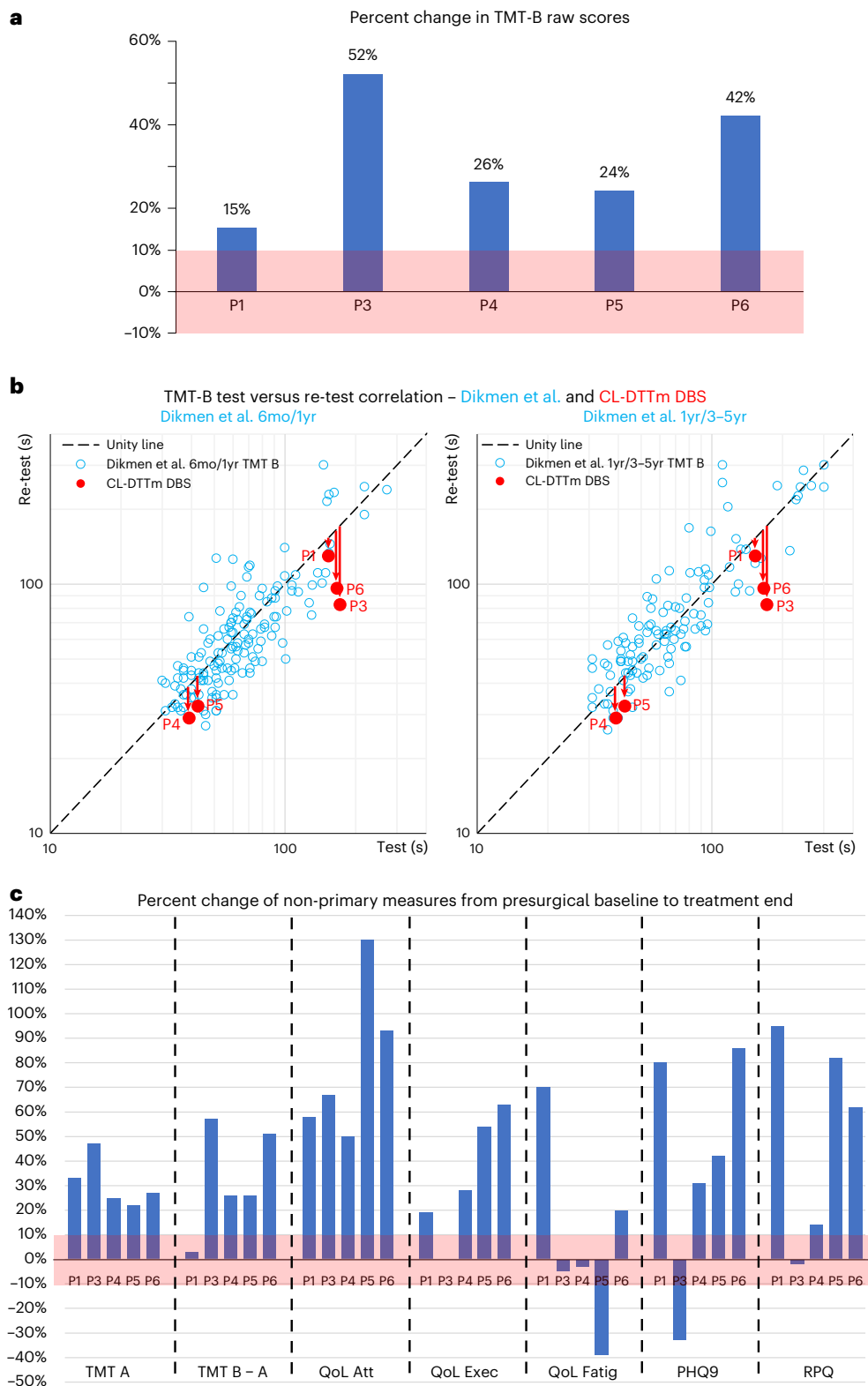


Fig. 2 | Behavioral results. a, TMT-B raw scores for each participant. Red line indicates the 10% improvement level, the preselected benchmark. **b**, Test–retest scattergram. Scattergram of data from two groups of msTBI participants (blue dots) followed as part of the Dikmen et al.⁵ study with available TMT-B measurements at time points (left panel) ($n = 146$) 6 months post-injury and again 1 year post-injury and (right panel) ($n = 118$) those who were followed 1 year post-injury and again between 3 and 5 years post-injury (provided by Dr. Dikmen) together with the five msTBI participants studied here (red dots). The CL/DTTm participants cluster on the lower edge of the ‘natural recovery’ group distributions. Statistical tests demonstrate that it is unlikely that the

CL/DTTm DBS participant values have been drawn from either of the ‘natural recovery’ distributions: $P < 0.02$ K–S test, one-sided ($P = 0.011$) (a) and $P < 0.005$ K–S test, one-sided (0.004070) (b). **c**, Percent change of non-primary measures from presurgical baseline to treatment end. All non-primary measures obtained across all five participants completing the study are shown. Improvement on measure is indicated by a positive change in percentage; worsening is indicated by a negative change in percentage (Supplementary Information). For Ruff 2&7 measures, complete presurgical data were only available for four participants (Supplementary Table 1).

(especially true for the bottom active contacts) across participants (Extended Data Table 2), suggesting greater inter-subject consistency of activating the same fiber system in the left hemisphere. The clustering of the active contacts shown in Fig. 5e,f demonstrates that the targeting methods used here (Fig. 3 and Extended Data Figs. 3–7) to identify the outflow of fibers from the lateral wing of CL into the DTTm are consistent across participants despite the wide variation in atrophy evident in this group (Extended Data Fig. 8 and Supplementary Figs. 12–17). As seen in Supplementary Video 2, the right-sided lead placements showed greater variance in tip placement than at the top contacts used for activation in the trial. Of note, despite the lack of activation of CL/DTTm in the activation modeling for P4's right hemisphere, both of P4's hemispheres show evoked potentials of comparable time course and spatial localization in the frontal cortex. This indicates that P4 received therapeutic stimulation in both hemispheres.

Comparison of TMT-B performance results with two cohorts studied by Dikmen et al. To estimate the likelihood that an average change in TMT-B completion time of this magnitude could occur spontaneously, we compared our results with those obtained from two subgroups of patients with msTBI who were followed by Dikmen et al.⁵ at (1) ($n = 146$) 6 months post-injury and again 1 year post-injury (a test–retest interval comparable to the present study) and (2) ($n = 118$) who were followed 1 year post-injury and again between 3 to 5 years post-injury (a time since injury comparable to the present study). Test–retest improvement of the five participants in our study contrasts significantly with the natural history changes documented by Dikmen et al. in both subgroups (Fig. 2b). In our sample, TMT-B completion times improved 15 to 52% from presurgical baseline to treatment end. In comparison, test–retest changes in the 6-month to 1-year Dikmen et al.⁵ sample were on average improved in TMT-B raw performance by <4% (the difference between our study and this cohort is significant at $P < 0.02$ ($P = 0.011$), Kolmogorov–Smirnov (K–S) test). For the 1-year to 3–5-year subgroup, the test–retest changes in the Dikmen et al.⁵ sample were on average (geometric mean) 4% slower ($P < 0.005$, K–S test (0.0041)); Supplementary Information provides comparisons with TMT-A and TMT-B minus TMT-A.

Discussion

We found that CL/DTTm DBS improved executive function as assayed by our primary outcome measure (TMT-B, which assesses attentional control), related performative tests (TMT-A, TMT-B minus TMT-A) and independent quality-of-life assessment instruments (TBIQoL-Attention and TBIQoL-Executive Function). Although variable across participants, we also observed improvements on the secondary outcome measures addressing fatigue, psychological health and global level of function. None of the participants met the benchmark for decline on the primary outcome measure and only one participant (P5) did so on the secondary outcome measure.

One of the goals of this study was to develop a detailed surgical planning procedure for accurately targeting the CL thalamic nucleus

at a specified angle of alignment designed to optimize stimulation of the fiber tract associated with CL (DTTm)^{19,29,30}. To do this we innovated a preprocessing pipeline (Supplementary Fig. 1) that included use of white-matter-nulled MRI, automated thalamic segmentation, DTI and biophysical modeling of applied electric fields. While we cannot be certain that all these steps were necessary, we can say that the targeting strategy used in this work differs markedly from previous DBS-targeting methods. Our findings shown in Supplementary Figs. 12–17 demonstrate that despite the wide range of brain atrophy and hemispheric asymmetries across our participants, use of the preprocessing pipeline and positioning and alignment within CL/DTTm resulted in a tight clustering of active electrode contacts within the synthetic atlas thalamus. These results support our interpretations below that the observed electrophysiological and behavioral effects reflect bi-hemispheric activation of the human CL/DTTm in the participants.

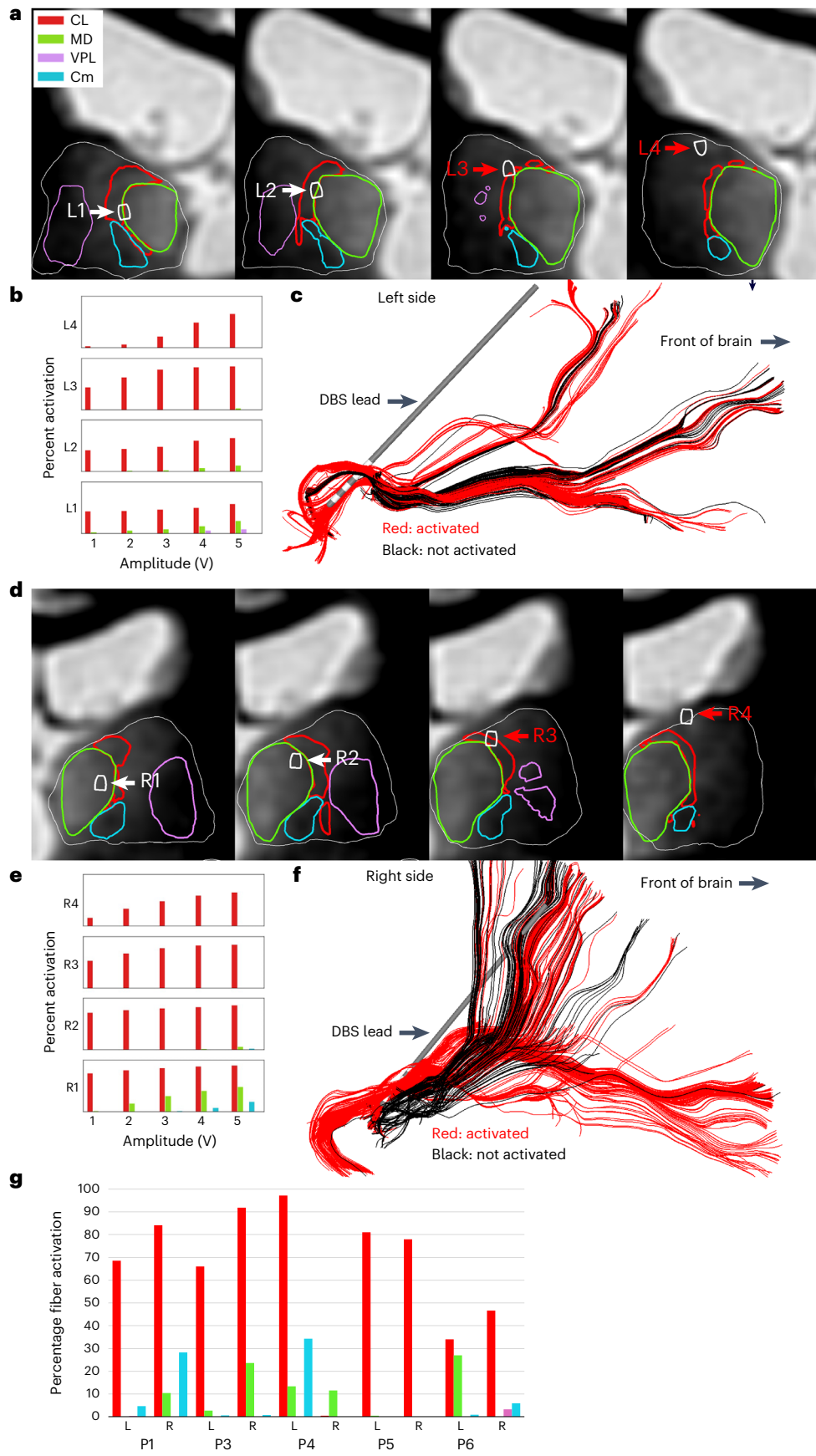
The preselected primary outcome measure, TMT-B, improved after 3 months of CL/DTTm DBS in all five participants who completed the trial (average 31.7% reduction in speed of performance). Of note, this finding was observed in people with chronic disability (≥ 2 years post-injury) caused by moderate-to-severe TBI. Baseline performance on the TMT-B ranged from severely impaired to the upper limits of the normal range. These results thus comport with improvements in both performance accuracy and reaction times observed in intact nonhuman primates carrying out executive task during CL/DTTm DBS^{19,29}. Several related measures capturing performative and qualitative aspects of executive attention also showed marked improvement, including TMT-A performance (average 30.7%), Trails B-A time (average 32%), TBIQoL-Attention (average 79.5%), and TBIQoL-Executive Function (average 32.7%). Despite the wide range of baseline scores noted on the TMT-B, performance improved by an average of approximately one s.d. (~ 10 units of T-score) on both TMT-B and TMT-A, based on demographically adjusted T-scores (Extended Data Table 1). The T-scores reflect population norms and this effect size is considered a clinically meaningful change³⁵. These findings contrast with the large observational study of msTBI of Dikmen et al.⁵

To test the robustness of our conclusions, we compared our cohort to two cohorts in that study, one comparable in test–retest interval and one comparable in duration since injury. We find that our effect sizes demonstrate significant improvement over that seen in both control groups (Fig. 2b and Supplementary Figs. 18 and 19). Our sample also demonstrated complementary improvements in self-reported attentional (TBIQoL-Attention) and executive (TBIQoL-Executive) functions associated with real-world behavioral competencies and subjective ratings of quality of life^{2–7,38}. These results are further supported by a parallel study involving these participants and their paired family members who underwent qualitative interviews and reported many real-world impacts enabled by these improvements (Supplementary Table 8 and refs. 36,37).

We interpret our findings of improved executive attention as the result of activating the CL/DTTm axonal projections (originating primarily from CL neuronal cell bodies) to partially deafferented

Fig. 3 | Activation of CL/DTTm fibers in a representative participant and group summary. **a**, Coronal WMn slices from the left hemisphere of participant P5, zoomed in to include only the left thalamus and lateral ventricle. Four slices are shown: each intersects the middle of one of the four DBS electrode contacts. The two active contacts L3 and L4 (used as cathodes during stimulation) are indicated by red labels and arrows. The intersection of each slice with the outer boundary of four 'key' thalamic nuclei is indicated by the color contours: CL (red), MD (green), VPL (purple) and Cm (cyan). **b**, Histograms of fiber activation from left hemisphere of participant P5, for each of the four DBS contacts driven at five different voltages from 1 V to 5 V, for CL, MD, VPL and Cm fibers. **c**, Modeled activation of P5's left hemisphere CL/DTTm fibers (active fibers rendered in red, inactive fibers rendered in black). **d**, Coronal WMn slices from the right hemisphere of participant P5, zoomed in to include only the right thalamus

and lateral ventricle. Four slices are shown: each intersects the middle of one of the four DBS electrode contacts. The two active electrode contacts R3 and R4 (used as cathodes during stimulation) are indicated by red labels and arrows. The intersection of each slice with the outer boundary of four 'key' thalamic nuclei is indicated by the color contours: CL (red), MD (green), VPL (purple) and Cm (cyan). **e**, Histograms of modeled fiber activation from right hemisphere of participant P5, for each of the four DBS electrode contacts driven at five different voltages from 1 V to 5 V, for CL, MD, VPL and Cm fibers. **f**, Modeled activation of P5's right hemisphere CL/DTTm fibers (active fibers are rendered in red; inactive fibers are rendered in black). **g**, Percent of fiber activation of target and avoidance fibers, all five participants. Color scheme is the same as in **a**, **b**, **d** and **e**, CL (red), MD (green), VPL (purple) and Cm (cyan).



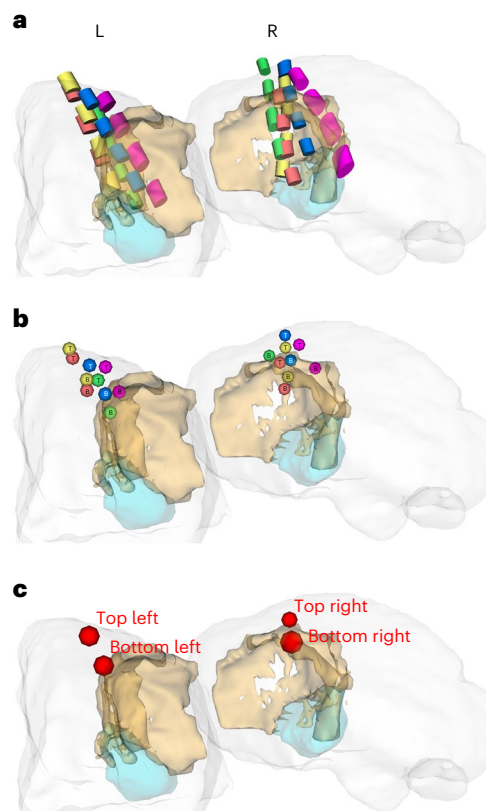


Fig. 4 | Placement and visualization of DBS contacts in common template space. **a**, CL and Cm. Three-dimensional (3D) rendering of CL (light brown) and Cm (cyan) nuclei within the thalamus (transparent gray). Postoperative electrodes. Rendering of the four DBS electrodes for each of the five participants, color-coded by participant as follows: P1 (yellow), P3 (salmon), P4 (green), P5 (blue) and P6 (magenta). These electrode renderings indicate the final postoperative locations, as determined by 30-d postoperative computed tomography (CT) scanning, and like all other panels in this figure, these locations have been warped into common template space. **b**, Active contacts identified. Small spherical renderings are shown within two of the DBS electrodes on each of left and right sides, to indicate that these are the two (top and bottom) active contacts used during stimulation of this participant. Note that the top active contact on the right side for P4 (green) was shorted as a result of this contact being fully outside the thalamus and in the cerebrospinal fluid (CSF) of the lateral ventricle. For this reason, this contact could not be used during stimulation and is therefore not shown in this panel, nor was it used for the computation of centroids. **c**, Active contact centroid spheres. Centroids of top and bottom contacts computed across the five participants, and rendered as red spheres, with location of the sphere showing the 3D location of the centroid and the diameter of the sphere set equal to the s.d. (spatial spread) across the five participants, providing a graphical indication of the tightness-of-clustering of top and bottom active contacts in common space, in relation to CL and outer surface of thalamus.

neurons across Brodmann areas 6/8 (premotor, pre-SMA/SMA/FEF), 24 (anterior cingulate), 46 (dorsolateral prefrontal) and the rostral striatum. These regions have demonstrated monosynaptic connections with CL in rodents and nonhuman primates^{39–41}. The centering of evoked fields between lateral and medial frontal cortical regions (Fig. 5 and Supplementary Figs. 2–11) is consistent with these anatomical connections; however, we note that the evoked response profiles cannot resolve local cortical regional activations although future analyses with source localization methods might add further detail. Clinical and neuroimaging studies of msTBI participants link their functional neuropsychological impairments, including impaired TMT-B performance, to initial deafferentation severity^{5,7,9} and loss

of corticostriatal connectivity^{14–16}, specifically loss of connections of medial frontal cortical regions, including the anterior cingulate cortex^{14,15}, pre-supplementary motor area (pre-SMA) and superior frontal gyrus¹⁶ with the striatum. The pre-SMA and rostral striatum are critical regions that facilitate decision-making under time pressure⁴² and are both heavily innervated by CL afferents^{21,40}. A study of structural MRIs in 157 msTBI participants¹⁸ identified two key observations relevant to our findings: widespread brain atrophy is typical after only 6 months following msTBI and observed persistent impairment in executive function is associated only with atrophy of the thalamus in the dominant left hemisphere. As we achieved greater consistency of placement of the electrode in the left hemisphere as shown in the synthetic atlas results (Fig. 5) and more consistently localized cortical activations with activation of left-hemisphere electrode contacts (Fig. 5), our results may predominantly reflect compensation for left-hemispheric dysfunction. Our participants, however, like the broader msTBI population¹⁸ demonstrate bilateral atrophy and varying degrees of multifocal cerebral injury (Supplementary Figs. 12–17).

The primary effects of CL/DTTm stimulation as assessed by the TMT-B likely depend on activation of large, myelinated axons within CL/DTTm per se perhaps with contribution from additional axons of cells within closely positioned paralaminar regions of the median dorsalis nucleus⁴³. Cell bodies within the ‘lateral wing’ of CL⁴³ project to the rostral striatum and prefrontal/frontal cortical regions^{39–41,43}. In intact nonhuman primates, stimulation of CL/DTTm facilitates executive attention in intact animals¹⁹; conversely, a loss of the behavioral facilitation produced with CL/DTTm stimulation occurs when stimulation combines activation of nearby Cm projections passing through the thalamic reticular nucleus into the DTTm bundle²⁹. This experimental observation is also consistent with our findings that transient sensory and other side effects emerged in several participants when stimulating via the lower contacts, which were within or near Cm (Supplementary Information). Recent experimental studies have also shown that stimulation of CL is selectively effective to emerge nonhuman primates from general anesthesia using both microstimulation methods²⁰ and macrostimulation methods that activate both CL and MD^{44,45}. Notably, VA/VL stimulation is experimentally non-effective⁴⁵, supporting our interpretation here that observed effects of upper contacts placed just outside the nuclear boundary of CL produce activation of CL/DTTm per se. Consistency of activation of DTTm fibers by the upper contacts (as shown in Figs. 3g and 4) supports the role of these contacts in further activation of CL outflow as opposed to local neuronal populations in VA/VL per se.

Neocortical neurons markedly change their firing patterns following even small increases in membrane potential depolarization⁴⁶. We propose that CL/DTTm DBS effectively increases the depolarization tone of frontostriatal neuronal membrane potentials across these cortical and subcortical populations and that these changes in membrane potential underlie the behavioral improvements observed here. As shown in Supplementary Figs. 12–17, all of our participants had dilatation of their ventricular systems along with cortical and subcortical atrophy, suggesting broad bi-hemispheric deafferentation of frontal and striatal neuronal populations. The partial deafferentation of these neurons resulting from msTBI can be expected to associate with reduced depolarization tone and lower average resting membrane potentials than those observed in the intact brain⁴⁶. The resulting increase in excitatory synaptic activity on monosynaptically connected neocortical and striatal neurons induced by CL/DTTm DBS (~150 Hz pulses for 12 h daily) likely increases membrane depolarization in these cells⁴⁷.

The marked shift in level of tonic input to neocortical neurons produced by CL/DTTm DBS may have a variety of effects: it may improve spatiotemporal integration within cortical pyramidal neurons, which is strongly influenced by overall background synaptic firing rates⁴⁸; it may trigger specific high-frequency thresholds for synaptic activity

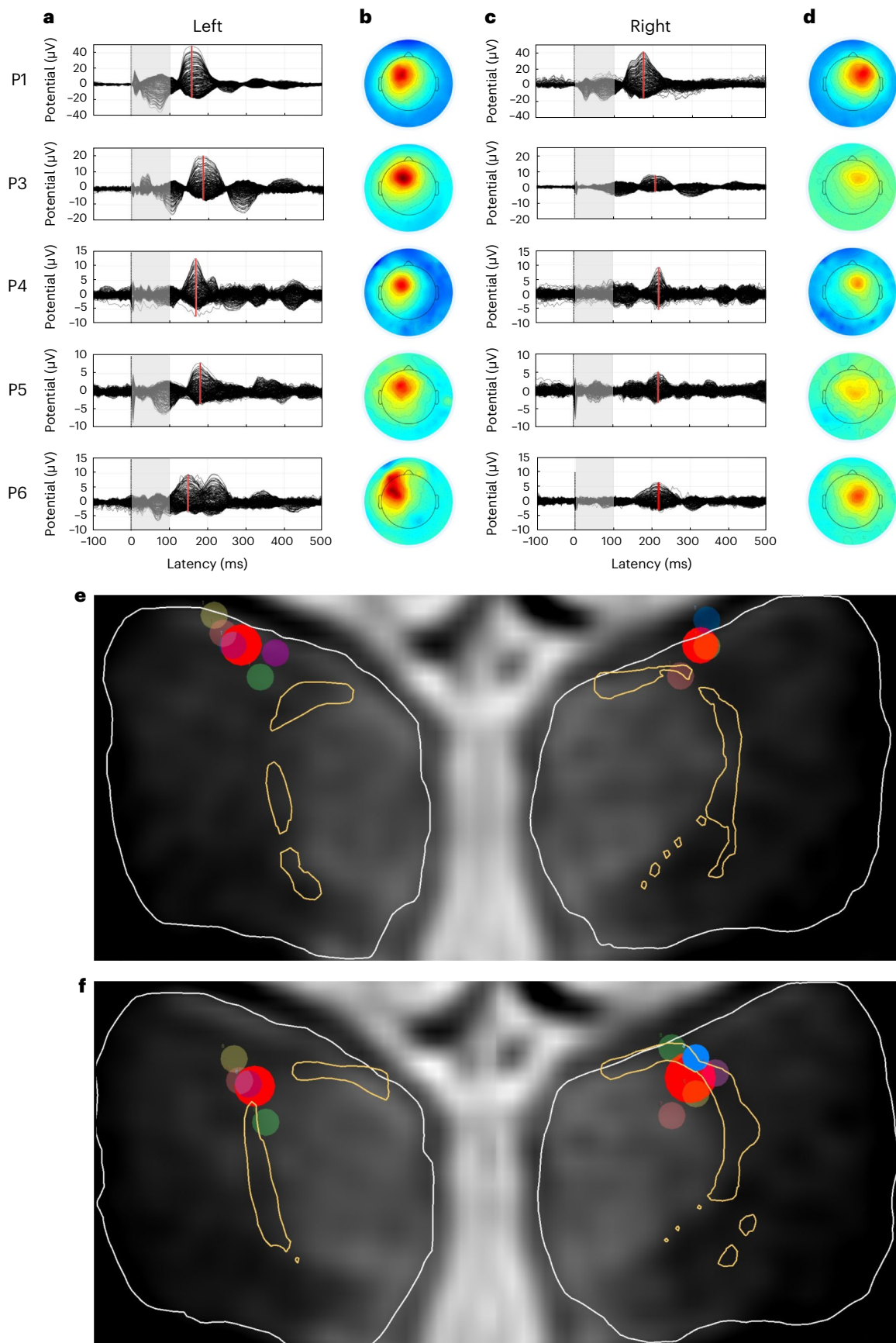


Fig. 5 | Cortical evoked responses for each individual from the left and the right hemisphere. a–d, DBS-evoked potentials obtained for the therapeutic contacts selected during the titration phase for treatment DBS for each participant (Supplementary Figs. 2–11). Stimulation was applied for the first 100 ms robust evoked potentials localized to the ipsilateral frontal cortex, with a peak amplitude between medial and lateral regions of frontal cortex noted in each panel. This is consistent with animal anatomical literature showing CL's strong connectivity to the dorsomedial frontal cortex^{39,40}. Evoked potentials in the left hemisphere demonstrate greater inter-subject consistency than those in the right hemisphere. As shown below (Fig. 4 and Extended Data Table 2),

right-sided bottom active contacts demonstrate greater variance in location potentially influencing this greater right-sided variability. **e,f**, Coronal slices through the common template WMn volume, zoomed to show thalamus and mid-line CSF only. Thin boundaries indicate the intersection of each slice with the THOMAS segmentations for CL (light brown) and whole thalamus (white). Small circles show the active contacts, color-coded for each participant similarly to those shown in Fig. 4, rendered as dim if out of plane or bright if in plane. Bright red larger circles indicate the intersection between the centroid spheres and the slice plane, with top active contacts and centroids (**e**) and bottom active contacts and centroids (**f**).

that in turn control a variety of mechanisms of dendritic electrogenesis in neocortical layers II, III and V^{49,50}; it may act at the network level as a high-frequency noise input to improve coincidence detection⁴⁹; and it may restore the dynamic range of neocortical neurons via gain control mechanisms that depend on synaptic background activity^{51,52}. Thus, restoration of depolarization tone is collectively expected to induce mechanisms that normalize integrative activity within frontal cortical and striatal neurons and, consequently, at the network level. In support of this notion, studies in intact nonhuman primates demonstrate that CL/DTM DBS produces changes at the network level by increasing the depth of task-related modulations of neuronal activity in frontostriatal neurons⁵³.

Notably, this mechanism can be directly tested in human participants in future studies: longitudinal increases of neuronal GABAergic tone (a physiological index of intraneuronal inhibitory tone) within frontostriatal neuronal populations in mTBI participants correlate with executive function providing support for the mechanism proposed here⁵⁴. Increasing arousal regulation within wakeful states is primarily associated with increasing inhibitory tone within cortical neurons⁴⁷; CL/DTM DBS-induced reversal of a selectively downregulated GABAergic signal across these structures in association with TMT improvements is a sharp prediction of our results.

Our study has several limitations. The main limitation is that, while the effect size on the primary outcome measure, TMT-B, is large (in that we find TMT-B improvements significantly exceed those observed in a comparable natural recovery cohort at time points after 6 months), the number of participants is small. The study is also underpowered to address many important questions that depend on between-participant comparisons, including how observed effects on performative tests may interact with lesion site and mechanism and how changes in self-report measures may reflect unmeasured psychosocial and economic factors. Additionally, our small sample does not allow assessment of how variations in treatment (precise electrode position and orientation in each hemisphere relative to the CL/DTM target and target avoidance fibers) impact efficacy. Additional limitations include the incompleteness and variability of the planned blinded withdrawal phase, and the short timeframe of the study. The 3-month treatment phase limits any systematic evaluation of long-term changes, management and psychosocial impacts of the invention. A direct test of generalizability of our findings will require a randomized clinical trial with a large number of participants studied with the same precision of targeting methods and verification of relative isolation of stimulation of the CL/DTM. Another important limitation is the choice of TMT-B as the sole outcome measure to capture impaired executive attention and related aspects of executive function; future work should develop composite measures to broaden the range of effects tested¹⁸.

Online content

Any methods, additional references, Nature Portfolio reporting summaries, source data, extended data, supplementary information, acknowledgements, peer review information; details of author contributions and competing interests; and statements of data and code availability are available at <https://doi.org/10.1038/s41591-023-02638-4>.

References

- Hammond, F. M. et al. Patterns of functional change five to ten years after moderate-severe traumatic brain injury. *J. Neurotrauma* **38**, 1526–1534 (2021).
- Wilson, L. et al. The chronic and evolving neurological consequences of traumatic brain injury. *Lancet Neurol.* **16**, 813–825 (2017).
- Finnanger, T. G. et al. Life after adolescent and adult moderate and severe traumatic brain injury: self-reported executive, emotional, and behavioural function 2-5 years after injury. *Behav. Neurol.* **2015**, 329241 (2015).
- Olsen, A. et al. Altered cognitive control activations after moderate-to-severe traumatic brain injury and their relationship to injury severity and everyday-life function. *Cereb. Cortex* **25**, 2170–2180 (2015).
- Dikmen, S. S., Machamer, J. E., Powell, J. M. & Temkin, N. R. Outcome 3 to 5 years after moderate to severe traumatic brain injury. *Arch. Phys. Med. Rehabil.* **84**, 1449–1457 (2003).
- Dikmen, S. S. et al. Cognitive outcome following traumatic brain injury. *J. Head. Trauma Rehabil.* **24**, 430–438 (2009).
- Draper, K. & Ponsford, J. Cognitive functioning ten years following traumatic brain injury and rehabilitation. *Neuropsychology* **22**, 618–625 (2008).
- Ruttan, L., Martin, K., Liu, A., Colella, B. & Green, R. E. Long-term cognitive outcome in moderate to severe traumatic brain injury: a meta-analysis examining timed and untimed tests at 1 and 4.5 or more years after injury. *Arch. Phys. Med Rehabil.* **89**, S69–S76 (2008).
- Lange, R. T., Iverson, G. L., Zakrzewski, M. J., Ethel-King, P. E. & Franzen, M. D. Interpreting the trail making test following traumatic brain injury: comparison of traditional time scores and derived indices. *J. Clin. Exp. Neuropsychol.* **27**, 897–906 (2005).
- Corrigan, J. D. et al. US population estimates of health and social outcomes 5 years after rehabilitation for traumatic brain injury. *J. Head. Trauma Rehabil.* **29**, E1–E9 (2014).
- National Academies of Science, Engineering and Medicine et al. In *Traumatic Brain Injury: A Roadmap for Accelerating Progress* (eds Matney, C., Bowman, K. & Berwick, D.) (National Academies Press, 2022).
- Tso, S., Saha, A. & Cusimano, M. D. The traumatic brain injury model systems national database: a review of published research. *Neurotrauma Rep.* **2**, 149–164 (2021).
- Iverson, G. L., Karr, J. E., Gardner, A. J., Silverberg, N. D. & Terry, D. P. Results of scoping review do not support mild traumatic brain injury being associated with a high incidence of chronic cognitive impairment: commentary on McInnes et al. 2017. *PLoS ONE* **14**, e0218997 (2019).
- De Simoni, S. et al. Altered caudate connectivity is associated with executive dysfunction after traumatic brain injury. *Brain* **141**, 148–164 (2018).
- Leunissen, I. et al. Task switching in traumatic brain injury relates to cortico-subcortical integrity. *Hum. Brain Mapp.* **35**, 2459–2469 (2014).

16. Leunissen, I. et al. Subcortical volume analysis in traumatic brain injury: the importance of the fronto-striato-thalamic circuit in task switching. *Cortex* **51**, 67–81 (2014).
17. Little, D. M. et al. Thalamic integrity underlies executive dysfunction in traumatic brain injury. *Neurology* **74**, 558–564 (2010).
18. Lutkenhoff, E. S. et al. The subcortical basis of outcome and cognitive impairment in TBI: a longitudinal cohort study. *Neurology* **95**, e2398–e2408 (2020).
19. Baker, J. L. et al. Robust modulation of arousal regulation, performance, and frontostriatal activity through central thalamic deep brain stimulation in healthy nonhuman primates. *J. Neurophysiol.* **116**, 2383–2404 (2016).
20. Redinbaugh, M. J. et al. Thalamus modulates consciousness via layer-specific control of cortex. *Neuron* **106**, 66–75 (2020).
21. Deschenes, M., Bourassa, J. & Parent, A. Striatal and cortical projections of single neurons from the central lateral thalamic nucleus in the rat. *Neuroscience* **72**, 679–687 (1996).
22. Ellender, T. J., Harwood, J., Kosillo, P., Capogna, M. & Bolam, J. P. Heterogeneous properties of central lateral and parafascicular thalamic synapses in the striatum. *J. Physiol.* **591**, 257–272 (2013).
23. Llinas, R. R., Leznik, E. & Urbano, F. J. Temporal binding via cortical coincidence detection of specific and nonspecific thalamocortical inputs: a voltage-dependent dye-imaging study in mouse brain slices. *Proc. Natl Acad. Sci. USA* **99**, 449–454 (2002).
24. Shirvalkar, P., Seth, M., Schiff, N. D. & Herrera, D. G. Cognitive enhancement with central thalamic electrical stimulation. *Proc. Natl Acad. Sci. USA* **103**, 17007–17012 (2006).
25. Liu, J. et al. Frequency-selective control of cortical and subcortical networks by central thalamus. *eLife* **4**, e09215 (2015).
26. Wyder, M. T., Massoglia, D. P. & Stanford, T. R. Contextual modulation of central thalamic delay-period activity: representation of visual and saccadic goals. *J. Neurophysiol.* **91**, 2628–2648 (2004).
27. Schiff, N. D. Recovery of consciousness after brain injury: a mesocircuit hypothesis. *Trends Neurosci.* **33**, 1–9 (2010).
28. Schiff, N. D. et al. Behavioural improvements with thalamic stimulation after severe traumatic brain injury. *Nature* **448**, 600–603 (2007).
29. Janson, A. P. et al. Selective activation of central thalamic fiber pathway facilitates behavioral performance in healthy non-human primates. *Sci. Rep.* **11**, 23054 (2021).
30. Edlow, B. L. et al. Neuroanatomic connectivity of the human ascending arousal system critical to consciousness and its disorders. *J. Neuropathol. Exp. Neurol.* **71**, 531–546 (2012).
31. Janson, A. P. & Butson, C. R. Targeting neuronal fiber tracts for deep brain stimulation therapy using interactive, patient-specific models. *J. Vis. Exp.* **138**, 57292 (2018).
32. Lannoo, E., Colardyn, F., Jannes, C. & de Soete, G. Course of neuropsychological recovery from moderate-to-severe head injury: a 2-year follow-up. *Brain Inj.* **15**, 1–13 (2001).
33. Wilson, L. et al. A manual for the Glasgow outcome scale-extended interview. *J. Neurotrauma* **38**, 2435–2446 (2021).
34. Sanchez-Cubillo, I. et al. Construct validity of the Trail Making Test: role of task-switching, working memory, inhibition/interference control, and visuomotor abilities. *J. Int. Neuropsychol. Soc.* **15**, 438–450 (2009).
35. Heaton, R. K., Walden Miller, S., Taylor, M. J. & Grant, I. *Revised Comprehensive Norms for an Expanded Halstead-Reitan Battery: Demographically Adjusted Neuropsychological Norms for African American and Caucasian Adults* (Psychological Assessment Resources, 2004).
36. Fins, J. J., Wright, M. S., Henderson, J. M. & Schiff, N. D. Subject and family perspectives from the central thalamic deep brain stimulation for traumatic brain injury study: part I. *Camb. Q Health. Ethics* **31**, 419–443 (2022).
37. Fins, J. J., Wright, M. S., Shulman, K. S., Henderson, J. M. & Schiff, N. Subject and family perspectives from the central thalamic deep brain stimulation for traumatic brain injury study: part II. *Camb Q Healthc. Ethics* (in the press).
38. Hart, T., Whyte, J., Kim, J. & Vaccaro, M. Executive function and self-awareness of ‘real-world’ behavior and attention deficits following traumatic brain injury. *J. Head. Trauma Rehabil.* **20**, 333–347 (2005).
39. Hsu, D. T. & Price, J. L. Midline and intralaminar thalamic connections with the orbital and medial prefrontal networks in macaque monkeys. *J. Comp. Neurol.* **504**, 89–111 (2007).
40. Morel, A., Liu, J., Wannier, T., Jeanmonod, D. & Rouiller, E. M. Divergence and convergence of thalamocortical projections to premotor and supplementary motor cortex: a multiple tracing study in the macaque monkey. *Eur. J. Neurosci.* **21**, 1007–1029 (2005).
41. Shook, B. L., Schlag-Rey, M. & Schlag, J. Primate supplementary eye field. II. Comparative aspects of connections with the thalamus, corpus striatum, and related forebrain nuclei. *J. Comp. Neurol.* **307**, 562–583 (1991).
42. Forstmann, B. U. et al. Striatum and pre-SMA facilitate decision-making under time pressure. *Proc. Natl. Acad. Sci. USA* **105**, 17538–17542 (2008).
43. Steriade, M. & Glenn, L. L. Neocortical and caudate projections of intralaminar thalamic neurons and their synaptic excitation from midbrain reticular core. *J. Neurophysiol.* **48**, 352–371 (1982).
44. Bastos, A. M. et al. Neural effects of propofol-induced unconsciousness and its reversal using thalamic stimulation. *eLife* **10**, e60824 (2021).
45. Tasserie, J. et al. Deep brain stimulation of the thalamus restores signatures of consciousness in a nonhuman primate model. *Sci. Adv.* **8**, eabl5547 (2022).
46. Steriade, M. Neocortical neurons are flexible entities. *Trends Neurosci.* **5**, 121–134 (2004).
47. Rudolph, M., Pelletier, J. G., Pare, D. & Destexhe, A. Characterization of synaptic conductances and integrative properties during electrically induced EEG-activated states in neocortical neurons in vivo. *J. Neurophysiol.* **94**, 2805–2821 (2005).
48. Bernander, O., Douglas, R. J., Martin, K. A. & Koch, C. Synaptic background activity influences spatiotemporal integration in single pyramidal cells. *Proc. Natl Acad. Sci. USA* **88**, 11569–11573 (1991).
49. Larkum, M. E., Zhu, J. J. & Sakmann, B. A new cellular mechanism for coupling inputs arriving at different cortical layers. *Nature* **398**, 338–341 (1999).
50. Larkum, M. E., Waters, J., Sakmann, B. & Helmchen, F. Dendritic spikes in apical dendrites of neocortical layer 2/3 pyramidal neurons. *J. Neurosci.* **27**, 8999–9008 (2007).
51. Khubieh, A., Ratte, S., Lankarany, M. & Prescott, S. A. Regulation of cortical dynamic range by background synaptic noise and feedforward inhibition. *Cereb. Cortex* **26**, 3357–3369 (2016).
52. Shu, Y., Hasenstaub, A., Badoual, M., Bal, T. & McCormick, D. A. Barrages of synaptic activity control the gain and sensitivity of cortical neurons. *J. Neurosci.* **23**, 10388–10401 (2003).
53. Baker, J. L. et al. Central thalamic deep brain stimulation enhances dominant spiking activity profiles of prefrontal and premotor cortical neurons in healthy and behaving non-human primates. In *5th Annual Minnesota Neuromodulation Symposium* (2018).
54. Kang, Y. et al. Longitudinal alterations in γ -aminobutyric acid (GABA(A)) receptor availability over approximately 1 year following traumatic brain injury. *Brain Commun.* **4**, fcac159 (2022).

Publisher's note Springer Nature remains neutral with regard to jurisdictional claims in published maps and institutional affiliations.

Springer Nature or its licensor (e.g. a society or other partner) holds exclusive rights to this article under a publishing agreement with

the author(s) or other rightsholder(s); author self-archiving of the accepted manuscript version of this article is solely governed by the terms of such publishing agreement and applicable law.

© The Author(s), under exclusive licence to Springer Nature America, Inc. 2023

¹Feil Family Brain Mind Institute, Weill Cornell Medicine, New York, NY, USA. ²Department of Neurology, Weill Cornell Medicine, New York, NY, USA. ³Department of Physical Medicine and Rehabilitation, Spaulding Rehabilitation Hospital, Boston, MA, USA. ⁴Department of Physical Medicine and Rehabilitation, Harvard Medical School, Boston, MA, USA. ⁵Scientific Computing and Imaging Institute Department of Bioengineering, University of Utah, Salt Lake City, UT, USA. ⁶Norman Fixel Institute for Neurological Diseases Departments of Neurology and Neurosurgery, University of Florida, Gainesville, FL, USA. ⁷Department of Neurosurgery, Stanford University, Stanford, CA, USA. ⁸Radiology and Radiological Sciences, Vanderbilt University, Nashville, TN, USA. ⁹Department of Population Health Sciences, Weill Cornell Medicine, New York, NY, USA. ¹⁰Department of Rehabilitation Medicine, University of Washington, Seattle, WA, USA. ¹¹Department of Medicine, Weill Cornell Medicine, New York, NY, USA. ¹²Department of Psychiatry, Stanford University, Stanford, CA, USA. ¹³Department of Computer Science, Stanford University, Stanford, CA, USA. ¹⁴Department of Radiology, Weill Cornell Medicine, New York, NY, USA. ¹⁵Department of Electrical Engineering, Stanford University, Stanford, CA, USA. ¹⁶Department of Neurological Surgery, University of Washington, Seattle, WA, USA. ¹⁷Department of Neuroimaging, University of Bordeaux, Nouvelle-Aquitaine, France. ¹⁸Neurological Institute, Cleveland Clinic, Cleveland, OH, USA. ¹⁹Department of Radiology, Stanford University, Stanford, CA, USA. ²⁰Wu Tsai Neurosciences Institute, Stanford University, Stanford, CA, USA. ²¹Bio-X Program, Stanford University, Stanford, CA, USA. ✉e-mail: nds2001@med.cornell.edu; henderj@stanford.edu

Methods

Participant recruitment

Participants were recruited through a variety of channels, including self-referral and provision of IRB-approved recruitment materials to academic research partners and consumer advocacy organizations serving patients with TBI. Recruitment materials identified the ClinicalTrials.gov number for the trial (NCT02881151). To accelerate enrollment, we also received IRB approval to subcontract with PatientWing (Philadelphia), a digital media marketing firm specializing in clinical trial recruitment. PatientWing identified potential study candidates using keyword searches on several online platforms including Google and various social media channels. To ensure equal access to our trial, PatientWing also launched a print campaign during the heavy holiday travel season in several Greyhound bus stations throughout California, targeting individuals without access to the internet.

Examiner training, certification and oversight procedures

Call center personnel from PatientWing were trained by key study staff (Drs Giacino and Kolakowsky-Hayner, licensed neuropsychologists) to conduct the telephone-based screening interviews. In addition, the neuropsychology staff conducted specialized training with five CITI (Collaborative Institutional Training Initiative) and HIPAA (Health Insurance Portability and Accountability Act)-certified research coordinators who were responsible for administration and scoring of the CT-DBS Multi-Dimensional Outcome Assessment Battery (see below). Training was conducted remotely using webinars and Zoom-based demonstrations. Examiners also completed the online training protocol required for administration, scoring and interpretation of the Columbia Suicide Severity Rating Scale. Following certification, all examiners received weekly virtual supervision by the licensed neuropsychologists. Separately scheduled troubleshooting meetings were held with research coordinators to address non-routine subject-specific issues and scoring ambiguities that arose in the context of test administration. GOS-E ratings were reviewed by key staff during team teleconferences to ensure accurate scoring and resolve ambiguities, which are commonly encountered on this measure.

Data quality assurance activities

Following development of the case report forms, we constructed a RED-Cap database consisting of 196 data elements. We created automated error-check functions that were monitored on an ongoing basis. Data were checked for missingness, errors and out-of-range or invalid values.

Ethical considerations and consent mechanisms

The research was carried out under a single IRB-approved protocol at Stanford University and participants gave written informed consent, according to CARE guidelines and in compliance with the Declaration of Helsinki principles. Supplementary Information provides additional information.

Study design

Eligibility criteria. Inclusion criteria. (1) History of moderate-to-severe TBI based on estimated GCS score within first 48 h of injury (acceptable GCS range, 3–12); (2) age 22–60 years; (3) at least 24 months from date of onset; (4) fluent in English and able to independently provide consent; (5) rating of lower moderate disability to lower good recovery on the GOS-E at the time of enrollment (acceptable GOS-E range 5–7); and (6) failure to return to pre-injury level of vocational or educational function.

The above criteria differed from those defined at the onset of the trial, which were: age 55 years maximum, GCS 9 maximum, GOS-E 6–7 and another criterion requiring a performance $\geq 2 \times$ s.d. below the demographically corrected mean on at least one attention, memory or executive function measure at baseline. All changes were approved by the US Food and Drug Administration amendment during the course of trial.

Exclusion criteria. (1) History of major developmental, neurologic, psychiatric or substance use disorder with evidence of disability before onset of TBI; (2) lesions involving two or more of the following regions: orbitofrontal, ventral prefrontal, mesial temporal and thalamus; (3) major medical comorbidities that, in the judgment of the PI, significantly increase risk or significantly reduce the likelihood of benefit from DBS; (4) malignancy with <5 years life expectancy; (5) untreated/uncontrolled (severe at the time of enrollment) depression or other psychiatric disorder; (6) women of childbearing age who do not regularly use an accepted contraceptive method (participants who become pregnant after enrollment may be excluded from the study and those who become pregnant before the surgical implantation of the DBS system will be excluded from the study); (7) inability to stop Coumadin or platelet anti-aggregation therapy before, during and after surgery; (8) previous DBS or other brain implants; (9) previous ablative intracranial surgery; (10) implantable hardware not compatible with MRI; (11) hardware, lesions or other factors limiting placement of electrodes in optimal target location in the judgment of the operating surgeon; (12) concurrent enrollment in any other clinical trial; and (13) any condition that, in the judgment of the PI, significantly increases risk or significantly reduces the likelihood of benefit from DBS.

Detailed clinical study design

Supplementary Table 10 contains a detailed description of study phases.

Statistical design

Descriptive statistics (for example, mean, median and percentage of change in raw and T-scores between time points) were calculated to summarize relevant participant characteristics. Both raw and T-score differences for behavioral measures were evaluated against a >10% cutoff that denoted improvement in each characteristic. SAS v.9.4 (SAS Institute) was used for all analyses.

Target localization

Image acquisition. In addition to a conventional scan protocol used for clinical presurgical DBS planning, participants were scanned with a WMn-MPRAGE protocol (WMn) protocol and a DTI protocol on a 3T GE MR750 scanner using a 32-channel head coil.

WMn image volumes were acquired using the following parameters: 3D MPRAGE sequence, coronal orientation, TE 4.7 ms, TR 11.1 ms, TI 500 ms, TS 5,000 ms, views per segment 240, FA 8°, receiver bandwidth ± 11.9 kHz, spatial resolution 1 mm isotropic, 220 slices per volume k-space ordering; two-dimensional radial fanbeam, ARC parallel imaging acceleration, 1.5×1.5 , scan time 8 min.

DTI image volumes were acquired using the following parameters: two-dimensional diffusion-weighted single-shot spin-echo echo planar imaging sequence, axial orientation, TE 74 ms, TR 8,000 ms, receiver bandwidth ± 250 kHz, diffusion directions: 60, diffusion weighting (b-value): 2,500 s mm⁻², spatial resolution 2 mm isotropic, 70 slices per volume, parallel imaging acceleration: 2, scan time 11 min.

WMn-MPRAGE and DTI image volumes were visually inspected to ensure that scans were of sufficient quality for analysis and were not corrupted by motion artifact.

Segmentation. Whole-brain WMn volumes were processed with the THOMAS thalamic segmentation tool with no preprocessing. The THOMAS algorithm applied to WMn images has been validated against manual segmentation⁵⁵. Using v.0 of this tool (github.com/sujason/thomas), we segmented and extracted the volumes of 12 lateralized structures in each hemisphere of the brain: whole thalamus, ten thalamic nuclei (anteroventral, Cm, lateral geniculate nucleus, MD, medial geniculate nucleus, pulvinar, ventral anterior, ventral lateral anterior, ventral lateral posterior and VPL), and one adjacent epithalamic structure, the habenula. Note that THOMAS segments the whole

thalamus separately from the thalamic nuclei; this whole thalamus encompasses all these preceding structures, as well as the mammillothalamic tract and some additional unlabeled thalamic areas (between segmented thalamic nuclei). In addition to THOMAS segmentation, we segmented the CL and ventral posteromedial (VPM) nuclei in each hemisphere using a single-atlas segmentation approach. This utilized manually-segmented CL and VPM nuclei, performed by a single expert neuroradiologist (T.T.) on the THOMAS template, which is an extremely high quality WMn brain volume formed by carefully registering and averaging 20 WMn volumes⁵⁵. The CL and VPM single atlases obtained this way were non-linearly warped to the WMn volumes of individual participants, and CL and VPM boundaries were finalized by trimming away any CL and VPM voxels that overlapped with THOMAS nuclei. In other words, THOMAS segmentations were allocated higher priority than CL and VPM segmentations, the rationale for this being that the THOMAS segmentations (obtained with a multi-atlas approach) were more accurate than the CL and VPM single-atlas segmentations.

DTI modeling. We used biophysical models to predict the degree of activation of fiber pathways seeded from several thalamic nuclei. Each pathway was created using deterministic tractography seeded from the following nuclei: Cm, CL, MD, VPL and VPM using DSI Studio ([dsi-studio. labsolver.org/](https://www.dsi-studio.com/)). Predictive models were created in SCIRun (<https://sci.utah.edu/software/scirun.html>) and used to predict the percent activation of each pathway via stimulation at each electrode across a range of amplitudes from -1 to -5 V. The results of these simulations were summarized in activation histograms that provided a visual summary of hundreds of individual simulations and allowed comparison of relative activation of pathways for targeting or avoidance.

Surgical planning for DBS electrode placement. We developed a new strategy for targeting the CL nucleus together with the fiber bundle of axons emanating from this region (DTTm)³⁰. Based on known monosynaptic connections determined in previous physiological and anatomical studies we sought to stimulate cell bodies and axonal regions with reciprocal connections to the 'lateral wing' of CL³⁰ and prefrontal/frontal cortical regions including anterior cingulate (area 24)³⁹, premotor, pre-supplementary motor/supplementary motor area (area 6)⁴⁰ and dorsomedial prefrontal cortex, including frontal eye fields (areas 8)⁴¹. In addition, we planned the DBS lead target and trajectory to stimulate fibers emanating from the paralaminar region of the medial dorsalis nucleus, which have strong projections to the dorsal lateral prefrontal cortex (area 46)⁵⁶. Collectively, the primary monosynaptic projections in the expected stimulation regions span the medial prefrontal/frontal regions with some extension over the lateral convexity of the frontal cortex.

To guide electrode placements to achieve this targeting of CL/DTTm we employed a three-step algorithm that involved a group consensus judgment at each step in the process to evaluate quality of evidence and model fidelity. Initial targets/trajectories were determined with relationship to (1) automated segmentations of thalamic sub-nuclei using THOMAS augmented by the CL/VPM single-atlas approach; (2) modeling of DTTm fibers emanating from each patient's individual CL shell volume using the DTI data subject to tractography using DSI Studio; and (3) biophysical modeling of fiber activation using model electrodes placed in the participant's brain space. Electrode placements were adjusted for safety and angle of entry point, consideration of local blood vessel anatomy and the maximal activation of the CL/DTTm fiber tract with minimal activation of off-target fibers (Fig. 3 and Extended Data Figs. 3–7).

Before selection of a final surgical trajectory for each patient's electrodes, patient-specific imaging, fiber tractography, segmented thalamic nucleus targets and bioelectric field models were incorporated into a planning simulation. This simulation facilitated optimization of each participant's lead trajectories based on 3D-segmented anatomical

targets and regions of avoidance, as well as finite element model (FEM) simulations predicting the outcome of a range of potential stimulation parameters. Team review of each separate stage of this algorithm resulted in selection of THOMAS model, DTI model and final chosen electrode positioning for presurgical planning.

The planning process, including lead positioning and bioelectric simulations, was performed using the open-source software project SCIRun. This software allowed MRI and CT imaging to be combined with patient-specific 3D models of thalamic nuclei created using the THOMAS segmentation algorithm. Lead placement models produced in SCIRun also included fiber tractography generated using the THOMAS nuclei as seed regions, which could be recolored following FEM simulations to represent fiber bundle activation in response to variable stimulation settings. A 3D representation of the Medtronic 3387 DBS lead was placed into each simulation and manipulated relative to AC–PC coordinates, allowing analogous trajectories to be explored both in Medtronic's StealthStation Surgical Navigation System and within the SCIRun model.

DBS lead placement was determined by a confluence of surgical safety considerations, investigated via the Stealth system, with anatomical targeting cues visualized within SCIRun. Special attention was given to placement of the electrode tip within the 'lateral wing' of the CL thalamic nucleus. This lateral wing was identified as the posterior projection of CL containing a bulk of its cellular somata as well as a majority of the efferent fiber tracts passing through the nucleus. To maximize activation of our targeted regions while avoiding activation of untargeted fibers, such as those projecting from Cm and VPL/VPM, electrodes were typically placed with their more proximal contacts outside of the body of CL, along the path of its projecting fibers (particularly those emerging from CL's lateral wing). This allowed for activation of CL-originating fiber tracts without requiring all active contacts to be embedded in the CL nucleus itself. Optimal lead placement required consideration of all the aforementioned elements within the SCIRun model, including the locations of cellular somata in each of the segmented thalamic nuclei as well as the shapes and projections of modeled fiber tracts.

Predicted activation of fiber tracts. Anatomical references (anterior and posterior commissures) and participant imaging assembled in SCIRun software were used to perform FEM simulations for each participant. FEM simulations provided insight for optimal surgical targeting as well as postoperative stimulation titration, with FEM-predicted activation serving as an initial guide for therapeutic stimulation parameter selection. These models were constructed using a simple activation function, calculated from the second derivative of stimulation voltage. Fiber tracts were 'activated' when activation function values within the fiber crossed a threshold, providing a percentage estimate of activation within the fiber bundle. Activated fibers can be 'painted' within the SCIRun model to provide a spatial representation of stimulation, for the purpose of comparing alternative lead positions and stimulation settings. The results of these simulations were also used to produce activation histograms, depicting the percentage of activation within five designated fiber bundles of interest.

Outlines of ideal DBS lead locations and thalamic nuclei of interest were embedded in MRI volumes by setting those regions' voxels to maximum intensity, then exporting them in DICOM format. These volumes were loaded into the surgical planning software (Stealth FrameLink, Medtronic) to facilitate final planning of lead trajectories.

Surgical targeting and implantation

Participants were admitted for 1–3 d following the surgical procedure and discharged when stable and ambulatory (Supplementary Information describes detailed surgical methods).

Postoperative programming

A postoperative CT with 0.5 mm³ voxels was acquired approximately 30 d after surgery. The purpose of this CT was to determine actual DBS

lead positions after any postsurgical pneumocephalus or brain shift had resolved. This postoperative image volume was co-registered with the preoperative MRI volumes using ANTS. DBS lead positions were determined by aligning the electrode contacts with the lead artifact in SCIRun. At this point the virtual monopolar review was repeated to assess activation of fiber pathways at a range of amplitudes. New histograms were generated and were used to guide the cathode survey during participant programming.

DBS electrode contact evoked potentials

EEG responses to DBS were recorded before the treatment phase in four out of five participants, with one participant (P3) needing to postpone recording until after the treatment phase due to COVID-related restrictions in place during the pretreatment time point. A high-density 256-channel EEG array (Electrical Geodesics) was placed on the scalp and NetStation Acquisition software (Electrical Geodesics) was used to record DBS-evoked potentials at a sampling rate of 1,000 Hz. DBS was delivered by the implanted neurostimulator and consisted of 3 min of 100-ms trains of square-wave pulses (60 μ s or 90 μ s per phase) with an inter-train interval of 2 s, delivered in a bipolar configuration across two contacts of the same lead. The amplitude and frequency of the stimulation trains were patient-specific (Supplementary Table 11). Recordings were obtained for every adjacent bipolar contact configuration for the left (E0+/E1-, E0-/E1+, E1+/E2-, E1-/E2+, E2+/E3- and E2-/E3+) and right (E8+/E9-, E8-/E9+, E9+/E10-, E9-/E10+, E10+/E11- and E10-/E11+) hemisphere leads.

Evoked potentials were identified by manually marking the starts of stimulation trains in the raw data using NetStation Review (Electrical Geodesics). This was conducted by a single investigator to eliminate inter-rater variability and checked by another investigator for accuracy. The 80–94 evoked potentials that were free of muscle artifacts were marked per bipolar contact configuration. Marked data were converted from the raw mff file format to the set file format accessible by EEGLAB v.2021.1 software (sccn.ucsd.edu/eeglab/index.php) run on MATLAB R2021a (The Mathworks). Briefly, the data were processed in EEGLAB as follows. Data were downsampled from 1,000 Hz to 250 Hz and filtered with a 1-Hz high pass filter. Line noise was then removed by the cleanLineNoise function of the EEG-Clean-Tools toolbox (PREP pipeline) v.0.56.0 (vislab.github.io/EEG-Clean-Tools)⁵⁷ and re-referenced to the average signal. EEG contacts with excessive artifacts were identified and their data removed (number of removed channels reported in Supplementary Table 13) and replaced by spherical interpolation by the clean raw data and pop_interp functions of EEGLAB. Data were re-referenced again to the average signal. A final cleaning step was conducted with independent component analysis. Independent components were identified using AMICA v.1.5 (sccn.ucsd.edu/~jason/amica_web.html) and labeled as brain signal, muscle artifact, eye movement, heart artifact, line noise, channel noise or ‘other’ using ICLabel v.1.3 (<https://github.com/sccn/ICLabel>). Muscle artifact, eye movement and channel noise components that were present at or greater than 50% in the data of EEG channels were removed (number of removed independent components are reported in Supplementary Table 13). Artifacts from blinks, cardiac activity and muscle contractions were removed by rejecting the corresponding sources from an independent-component analysis decomposition using the Infomax algorithm⁵⁸. Data then underwent a final re-reference to the average signal.

Cleaned data were epoched from –100ms to 500 ms, where 0 ms was the start of the 100 ms stimulation train and averaged to create a mean epoch for each bipolar contact configuration. Mean epochs from reverse polarity bipolar contact configurations (for example, E0+/E1- and E0-/E1+) were averaged together, creating a mean evoked potential map for each pair of adjacent contacts on a lead. This step was conducted to reduce the stimulation artifact and isolate the evoked potential⁵⁹. Mean bipolar evoked potential maps were plotted to examine the latencies and scalp locations of the evoked potentials (Supplementary Figs. 2–11).

Supplementary Figs. 2–11 show the DBS-evoked potentials obtained for the therapeutic contacts selected during the titration phase for treatment DBS for each participant. Overall, we observed robust evoked potentials localized to the ipsilateral frontal cortex, with the peak amplitude typically localized medially in the frontal cortex. This is consistent with animal anatomical literature showing CL’s strong connectivity to the dorsomedial frontal cortex. Evoked potentials in the left hemisphere were more robust than those in the right hemisphere. This is likely due to the implantation of the left electrode first and the right electrode second, which reduced the effect of brain shift on targeting. In general, across-patient plots showed an initial rapid low amplitude potential (~0–20 ms) likely corresponding to volume conduction of the DBS. This initial rapid low amplitude potential, with equally rapid decay, was localized to the ipsilateral side centered over the therapeutic contacts with the isolines demonstrating concentrated signal over the posteromedial frontal and anteromedial parietal cortices. The scalp electrode patterning for the initial potential was conserved across all patients.

Reporting summary

Further information on research design is available in the Nature Portfolio Reporting Summary linked to this article.

Data availability

A minimum dataset extracted from the REDCAP database has been made available on Dryad at <https://doi.org/10.5061/dryad.41ns1rmb>

References

- Su, J. H. et al. Thalamus Optimized Multi Atlas Segmentation (THOMAS): fast, fully automated segmentation of thalamic nuclei from structural MRI. *Neuroimage* **194**, 272–282 (2019).
- Mukherjee, A., Lam, N. H., Wimmer, R. D. & Halassa, M. M. Thalamic circuits for independent control of prefrontal signal and noise. *Nature* **600**, 100–104 (2021).
- Bigdely-Shamlo, N., Mullen, T., Kothe, C., Su, K. M. & Robbins, K. A. The PREP pipeline: standardized preprocessing for large-scale EEG analysis. *Front. Neuroinform.* **9**, 16 (2015).
- Bell, A. J. & Sejnowski, T. J. An information-maximization approach to blind separation and blind deconvolution. *Neural Comput.* **7**, 1129–1159 (1995).
- Baker, K. B., Montgomery, E. B. Jr., Rezaei, A. R., Burgess, R. & Luders, H. O. Subthalamic nucleus deep brain stimulus evoked potentials: physiological and therapeutic implications. *Mov. Disord.* **17**, 969–983 (2002).
- Laureys, S. & Schiff, N. D. Coma and consciousness: paradigms (re)framed by neuroimaging. *Neuroimage* **61**, 478–491 (2012).
- Purpura, K. P. & Schiff, N. D. The thalamic intralaminar nuclei: a role in visual awareness. *Neuroscientist* **3**, 8–15 (1997).
- Mair, R. G. & Hembrook, J. R. Memory enhancement with event-related stimulation of the rostral intralaminar thalamic nuclei. *J. Neurosci.* **28**, 14293–14300 (2008).
- Tabansky, I. et al. Temporally-patterned deep brain stimulation in a mouse model of multiple traumatic brain injury. *Behav. Brain Res.* **273**, 123–132 (2014).
- Shah, S. A., Baker, J. L., Ryou, J. W., Purpura, K. P. & Schiff, N. D. Modulation of arousal regulation with central thalamic deep brain stimulation. *IEEE Eng. Med. Bio.* **2009**, 3314–3317 (2009).
- Smith, A. C. et al. A Bayesian statistical analysis of behavioral facilitation associated with deep brain stimulation. *J. Neurosci. Meth.* **183**, 267–276 (2009).

Acknowledgements

Surgical implants (including leads and implantable neurostimulators) were provided by Medtronic. This work was supported by the National Institutes of Health BRAIN Initiative NINDS grant UH3 NS095554

(to N.D.S., J.T.G., C.R.B., E.Y.C., J.L.B., K.P.O., A.P.J., M.B., L.D., A.F., L.M.G., J.M., M.R., S.A.S., J.S., A.W., S.A.K.-H., J.J.F., A.G.M., B.K.R. and J.M.H.). J.C. and L.M.G. were partially supported by the following grant: Clinical and Translational Science Center at Weill Cornell Medical College (1-UL1-TR002384-01). The content is solely the responsibility of the authors and does not necessarily represent the official views of the National Institutes of Health. We thank the following personnel who supported this study: S. Taylor (Harvard/Spaulding); J. Lee (Weill Cornell); T. Prieto, H. Fortune, P. Rezaii, O. Rutledge, A. Bet, H.-B. Yeh, G. Qin, H. Fortune, T. Hornbeck, E. Lim (Stanford); S. Stanslaski, C. Zarns, N. Hopps, P. Stypulkowski (Medtronic); I. Korytov (Utah/Florida); D. Heyer (PatientWing); Biologics Consulting Group. We are grateful to S. Hwang for providing the artwork for Supplementary Fig. 1; L. Alkhoury for assistance with Extended Data Fig. 2; G. Iverson and C. Gaudet for discussion of practice effects in neuropsychological testing; and J. Whyte for comments on the manuscript.

Author contributions

N.D.S., J.M.H., J.T.G., C.R.B. and A.G.M. designed the study. J.M. acted as an independent consultation-liaison psychiatrist responsible for determination of decision-making capacity for each participant before study enrollment. J.T.G., N.D.S. and L.M.G. developed study design for outcome assessment. J.T.G., A.W., L.M.G. and J.C. analyzed behavioral data. S.D. and N.T. contributed supplementary data from University of Washington study and support in the use, analysis and interpretation of these data (Dikmen et al.). N.D.S. and J.D.V. designed and performed analysis of supplementary Dikmen et al.⁵ dataset. T.T., J.S., M.R. and B.K.R. developed the CL segmentation method. E.Y.C. and B.K.R. acquired neuroimaging data. E.Y.C., T.T., J.S., M.R., B.K.R., A.P.J., K.P.O. and C.R.B. designed and performed analysis of neuroimaging data. C.R.B., A.P.J. and K.P.O. designed and performed analysis of bioelectrical field modeling. E.Y.C., J.L.B. and S.A.S. developed the overall study design for neurophysiological data acquisition. E.Y.C. and J.L.B. designed cortical evoked potential experiments. E.Y.C., J.L.B. and M.K. analyzed cortical evoked potential data. L.D. coordinated the study components, US FDA regulatory compliance and patient recruitment liaison with PatientWing. J.J.F. developed ethical framework and guidance; PI of companion BRAIN Initiative study (1RF1MH12378-01) tracking participant and family perspectives which informed subject selection and enrollment. N.D.S. acted as

the administrative PI of UH3 grant. J.M.H. acted as physician sponsor of the US FDA Investigational Device Exemption and performed all surgical implants. H.M.B.S. provided neurophysiology acquisition and interpretation during surgical implants. N.D.S., J.M.H., J.T.G., C.R.B. and B.K.R. drafted the manuscript. All authors provided substantive feedback for revision of the manuscript.

Competing interests

The following authors are listed inventors on a patent application WO2023/043786 (jointly filed by Weill Cornell Medicine, University of Utah and Stanford University) describing detailed methods of integrating magnetic resonance imaging, biophysical modeling and electrophysiological methods for localization and placement of DBS electrodes in the CL/DTTm of the human thalamus as described in the manuscript: N.D.S., J.L.B., C.R.B., A.P.J., K.P.O., J.M.H., E.Y.C., B.K.R., J.S. and M.R. N.D.S., C.R.B. and J.L.B. are listed inventors on a related patent application WO2021/195062 (jointly filed by Weill Cornell Medicine, University of Utah). N.D.S. and J.L.B. are listed as inventors on US Patent 9,959,383 assigned to Weill Cornell Medicine describing different apparatus but related methods. The remaining authors declare no competing interests.

Additional information

Extended data is available for this paper at <https://doi.org/10.1038/s41591-023-02638-4>.

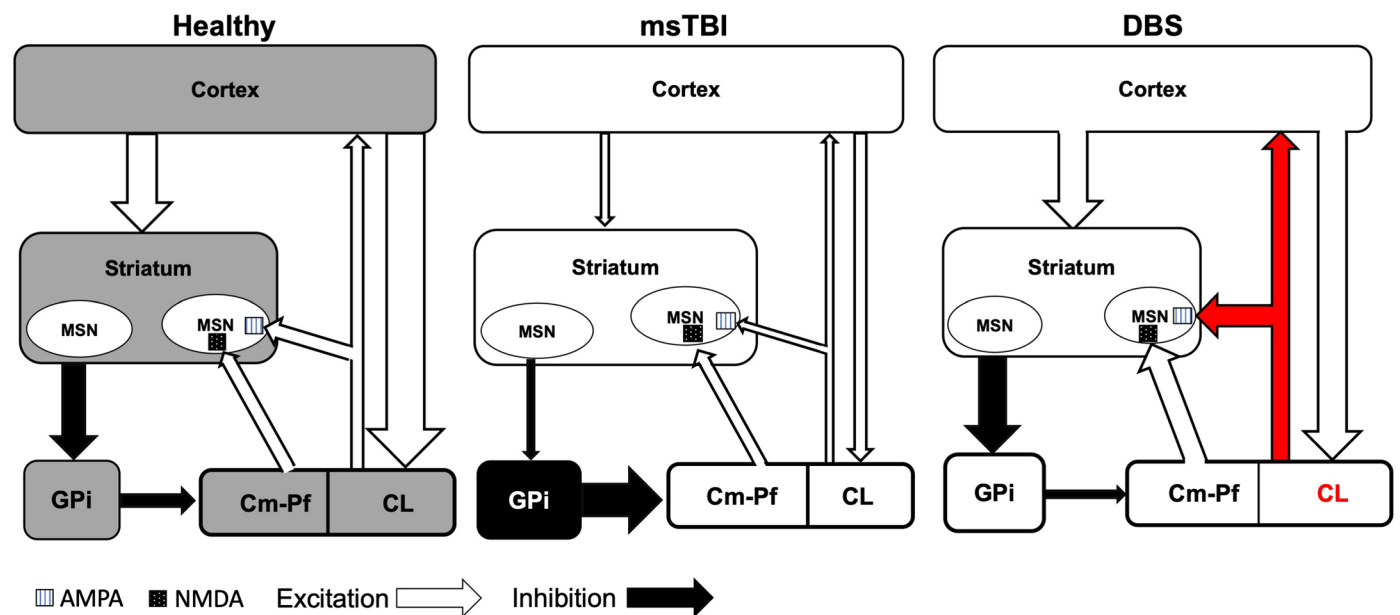
Supplementary information The online version contains supplementary material available at <https://doi.org/10.1038/s41591-023-02638-4>.

Correspondence and requests for materials should be addressed to Nicholas D. Schiff or Jaimie M. Henderson.

Peer review information *Nature Medicine* thanks the anonymous reviewers for their contribution to the peer review of this work. Primary Handling Editor: Jerome Staal, in collaboration with the *Nature Medicine* team.

Reprints and permissions information is available at www.nature.com/reprints.

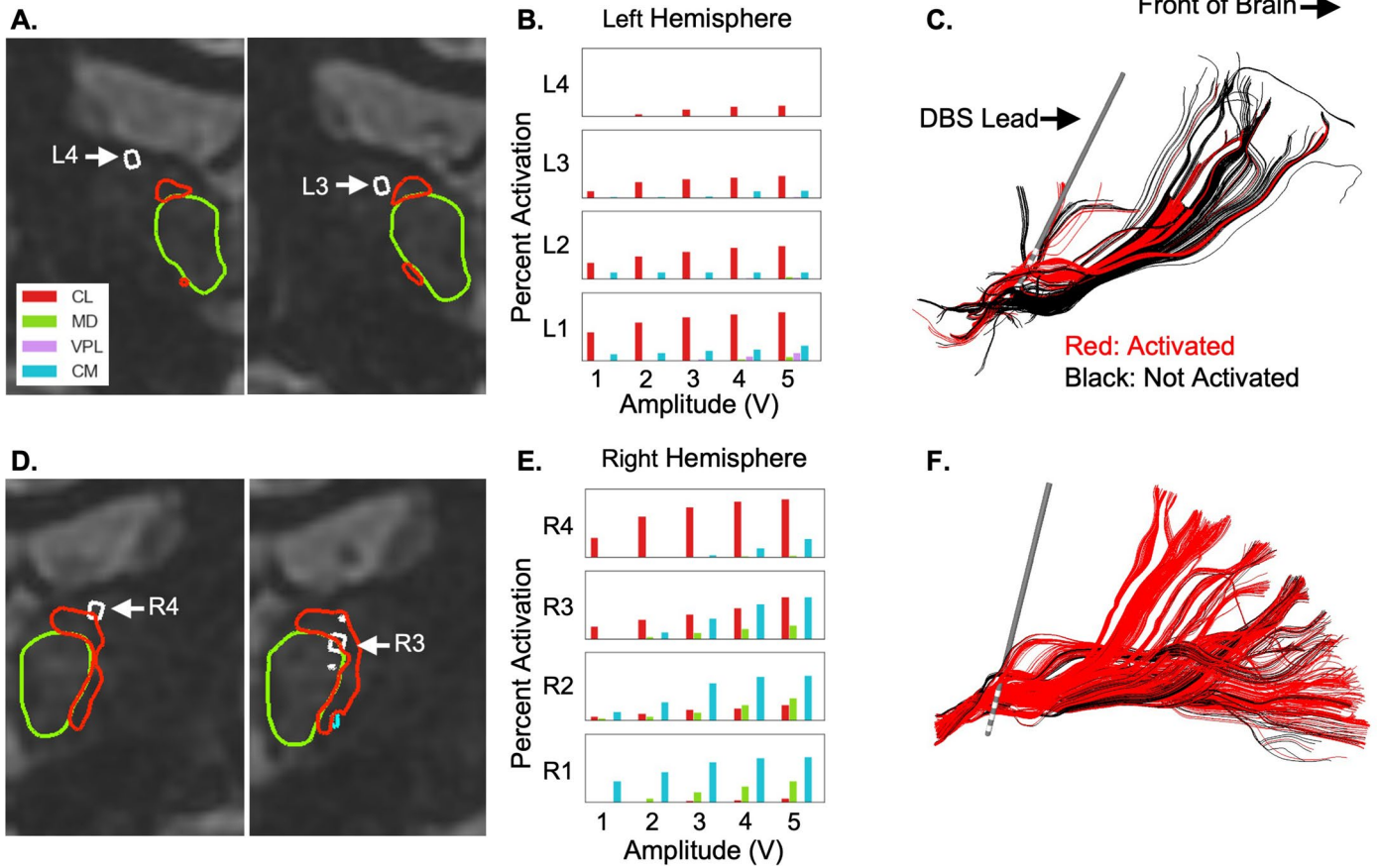
Theory: Mesocircuit mechanisms underlying CL/DTTm DBS impact on msTBI



Extended Data Fig. 1 | Mesocircuit theory for recovery of anterior forebrain function with CL/DTTm DBS in msTBI. Schematic diagram illustrating mesocircuit model for alteration of function following coma and moderate to severe brain injury and restoration of function with CL/DTTm DBS^{27,60}. **Left figure element:** Healthy normative function of corticothalamic system. Projections of central lateral thalamic neurons to anterior forebrain mesocircuit and posterior medial complex^{27,60}. CL co-activates frontal-parietal corticocortical connections and modulates their feed-forward and feedback connectivity via layer-specific effects within cortical columns^{20,60}. CL specifically targets supragranular and infragranular cortical layers avoiding projections into the input layers²³; these anatomical specializations support a proposed selective role in modulation of long-range corticocortical functional connectivity⁶¹. CL projections to the striatum strongly activate this structure via projections to medium spiny neurons, MSNs and act via AMPA receptors, whereas Cm-Pf afferents act via NMDA receptors²². **Middle figure element:** msTBI produces widespread deafferentation of the corticothalamic system leading to loss of CL modulation of cortex and striatum^{27,60}. Two major consequences of this downregulation of

CL output in combination with overall reduction of cerebral background activity are: 1) marked reduction in corticothalamic and corticostriatal outflow, 2) shut down of the medium spiny neuron output from striatum to globus pallidus interna (GPI) producing increased thalamic inhibition and further reduction of thalamocortical and thalamostriatal outflow. Collectively, these changes are proposed to exert a disproportionate impact on the anterior forebrain^{27,60}. **Right figure element:** CL/DTTm DBS is proposed to reverse the mesocircuit level effects of reduced corticothalamic, corticostriatal, and striato-pallidal output by direct overdrive pacing of CL output via the DTTm. This model for the effects of direct electrical stimulation of CL/DTTm in msTBI is supported by animal studies that demonstrate broad activation of the frontal cortex and striatum with CL electrical stimulation^{19,24,25}. These and related studies further show that CL electrical stimulation modulates executive attention and arousal in intact^{24,25,62} and brain-injured rodents⁶³, intact nonhuman primates^{19,29,61,64,65}, and a human subject in the minimally conscious state²⁸. Cortical evoked responses overlapping those observed here have been obtained in a human subject with CL DBS supporting the further generalizability of the findings²⁸.

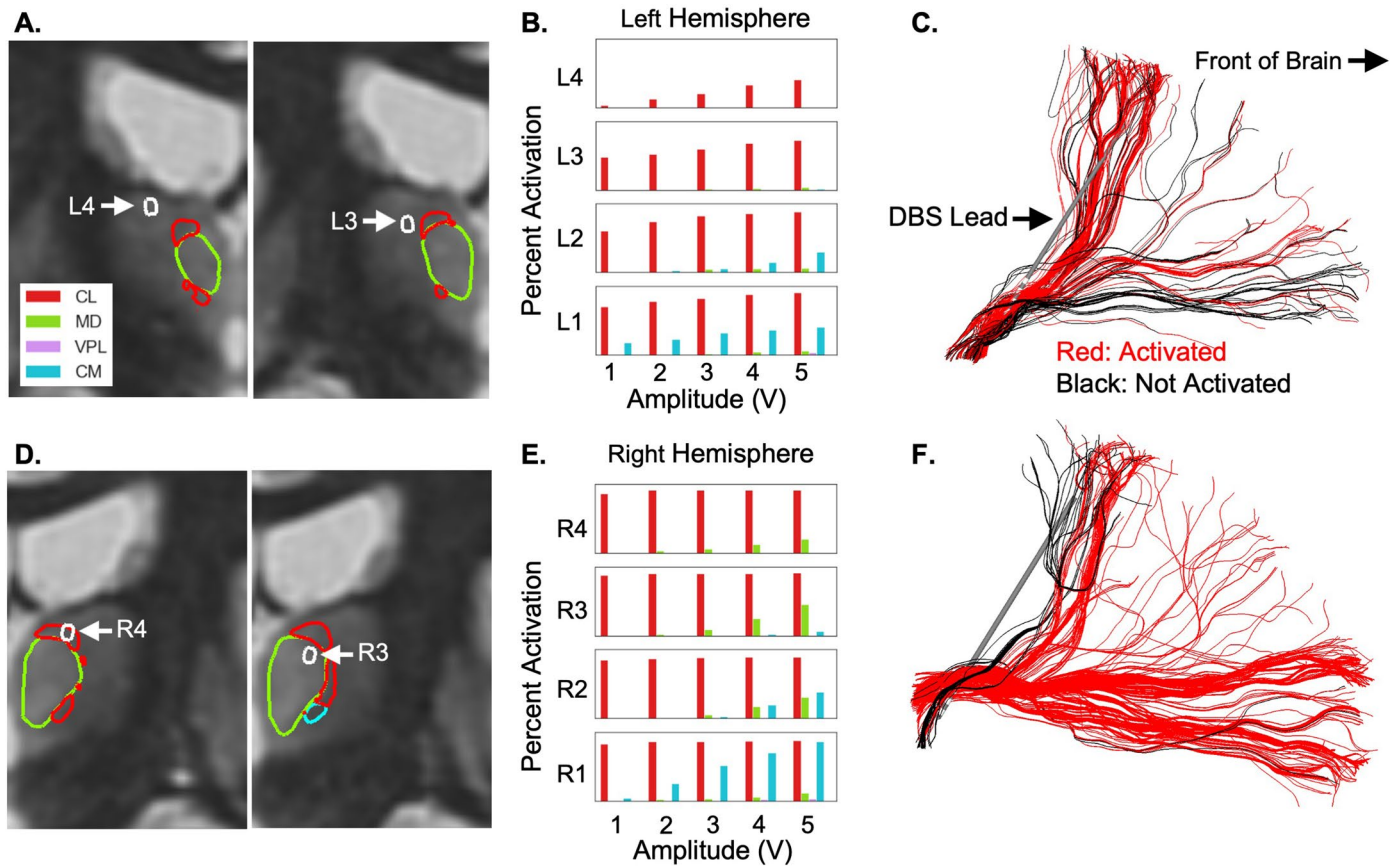
Participant 1 (P1)



Extended Data Fig. 3 | Placement of DBS electrodes within the CL/DTTm target for P1. **A.** Active contact locations and fiber bundles for left hemisphere of P1 rendered within P1 space, CL nucleus (red), MD (green), VPL (purple) Cm (cyan). **B.** Histograms of fiber activation for left sided CL, MD, VPL, and Cm. **C.** DBS activation of fibers (red), inactive fibers rendered in blue. **D.** Active

contact locations and fiber bundles for right hemisphere of P1 rendered within P1 space, CL nucleus (red), MD (green), VPL (purple) Cm (cyan). **E.** Histograms of fiber activation for right-sided CL, MD, VPL, and Cm. **F.** DBS activation of fibers (red), inactive fibers rendered in blue.

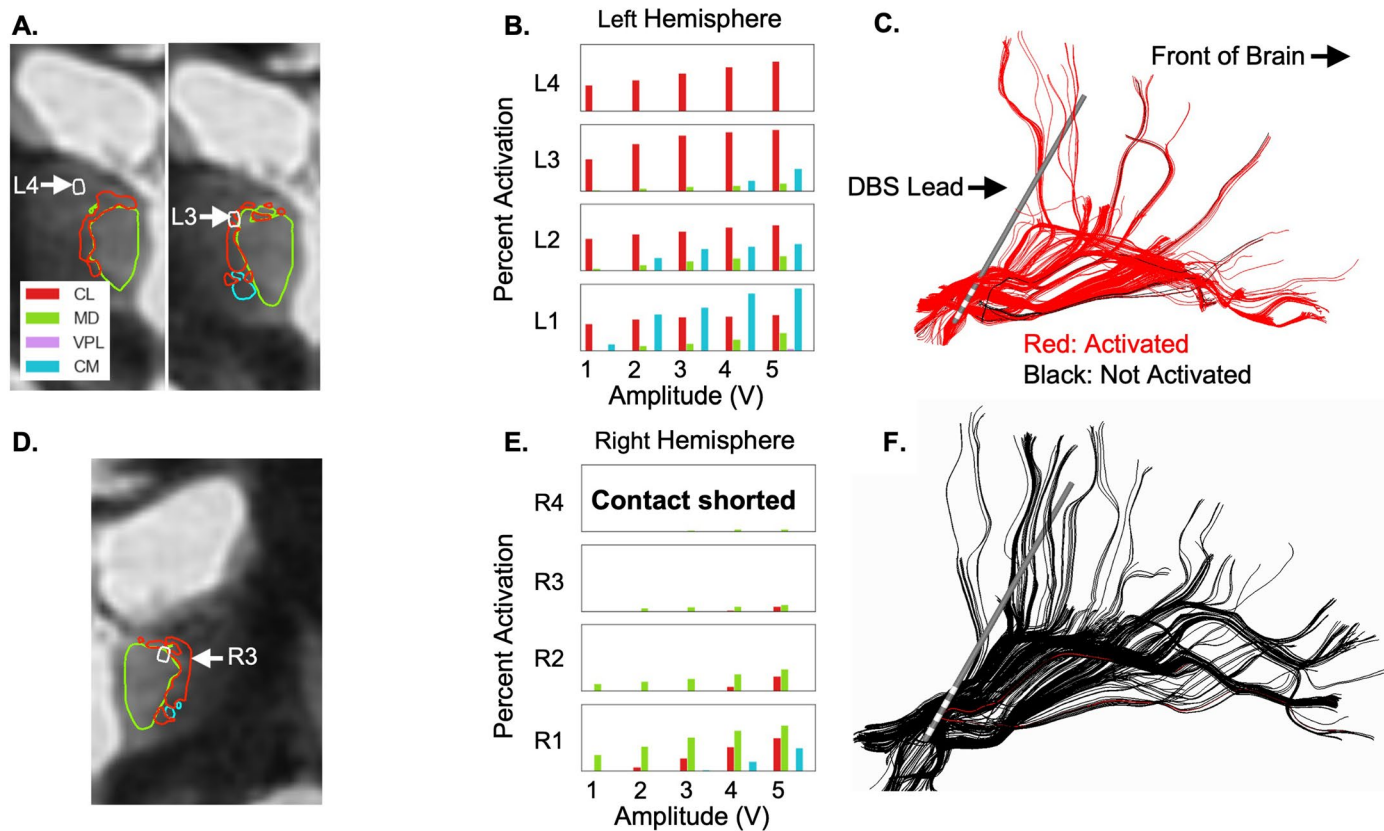
Participant 3 (P3)



Extended Data Fig. 4 | Placement of DBS electrodes within the CL/DTTm target for P4. **A.** Active contact locations and fiber bundles for left hemisphere of P3 rendered within P3 space, CL nucleus (red), MD (green), VPL (purple) Cm (cyan). **B.** Histograms of fiber activation for left sided CL, MD, VPL, and Cm. **C.** DBS activation of fibers (red), inactive fibers rendered in blue. **D.** Active

contact locations and fiber bundles for right hemisphere of P3 rendered within P3 space, CL nucleus (red), MD (green), VPL (purple) Cm (cyan). **E.** Histograms of fiber activation for right-sided CL, MD, VPL, and Cm. **F.** DBS activation of fibers (red), inactive fibers rendered in blue.

Participant 4 (P4)

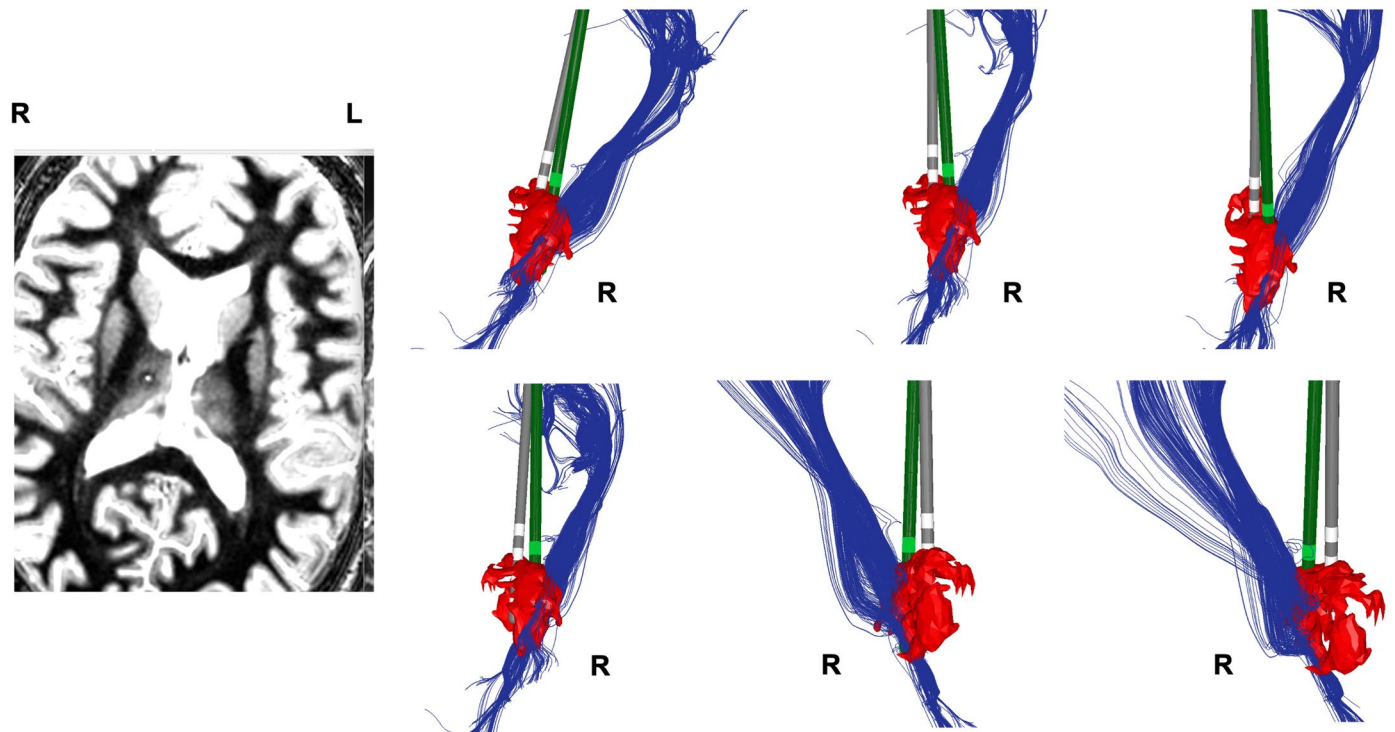


Extended Data Fig. 5 | Alteration of DTI model of CL/DTTm in P4 by local hemorrhage within right thalamus. A. Active contact locations and fiber bundles for left hemisphere of P4 rendered within P4 space, CL nucleus (red), MD (green), VPL (purple) CM (cyan). **B.** Histograms of fiber activation for left sided CL, MD, VPL, and Cm. **C.** DBS activation of fibers (red), inactive fibers rendered

in blue. **D.** Active contact locations and fiber bundles of P4 rendered within P4 space, CL nucleus (red), MD (green), VPL (purple) CM (cyan). **E.** Histograms of fiber activation for right-sided CL, MD, VPL, and Cm. **F.** DBS activation of fibers (red), inactive fibers rendered in blue.

Participant 4 (P4)

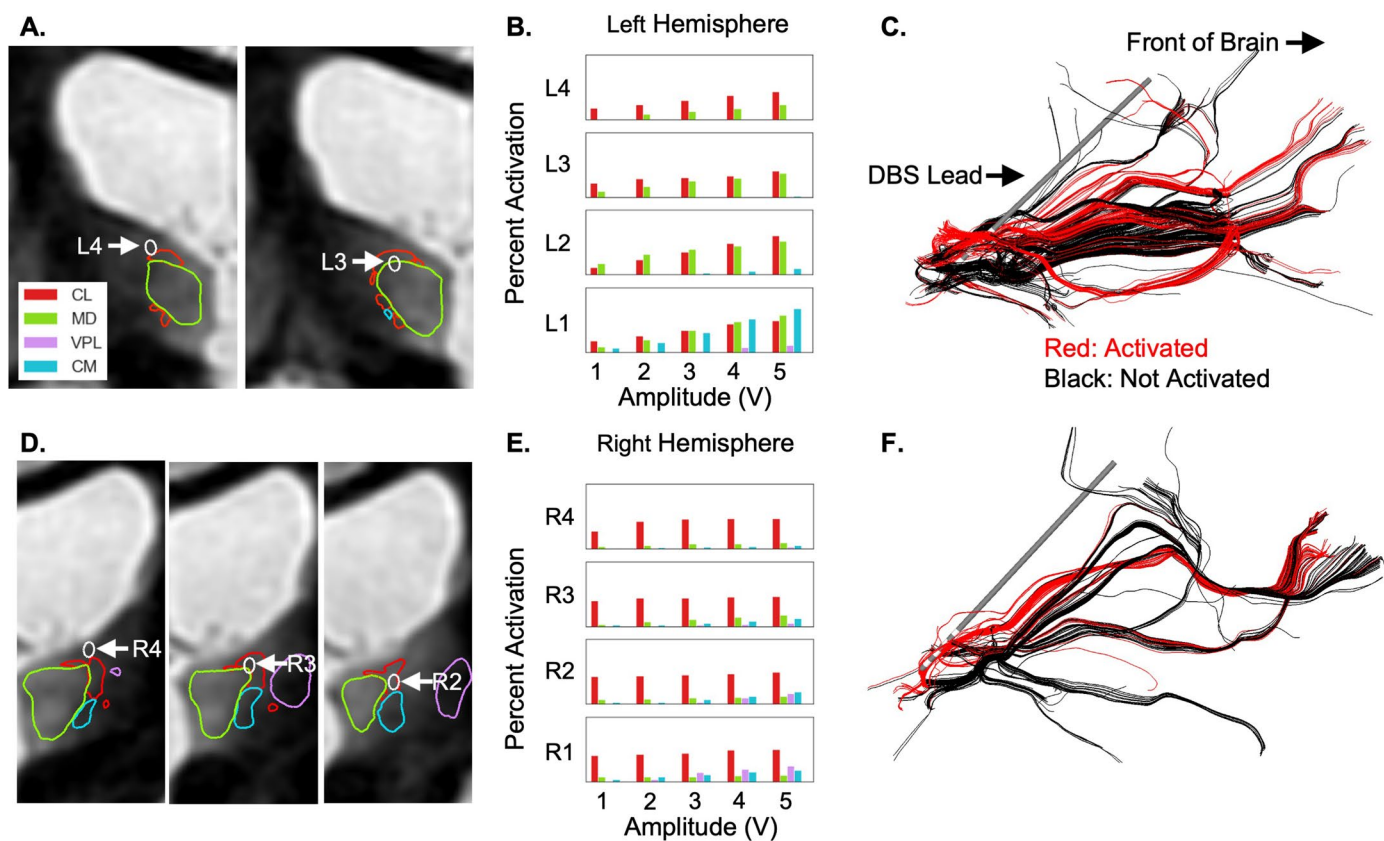
Comparisons of Pre-surgical planned and Post-surgical achieved electrode placements



Extended Data Fig. 6 | Alteration of DTI model of CL/DTM in P4 by local hemorrhage within right thalamus. MRI image shows large susceptibility artifact in the right central thalamus secondary to duret hemorrhage. Right panels: Distortion of MRI signal in this region limits the formation of DTI modeled fibers as seen in the six views comparing the presurgical locations of electrode placements (green electrode models) and postsurgical actual locations (gray

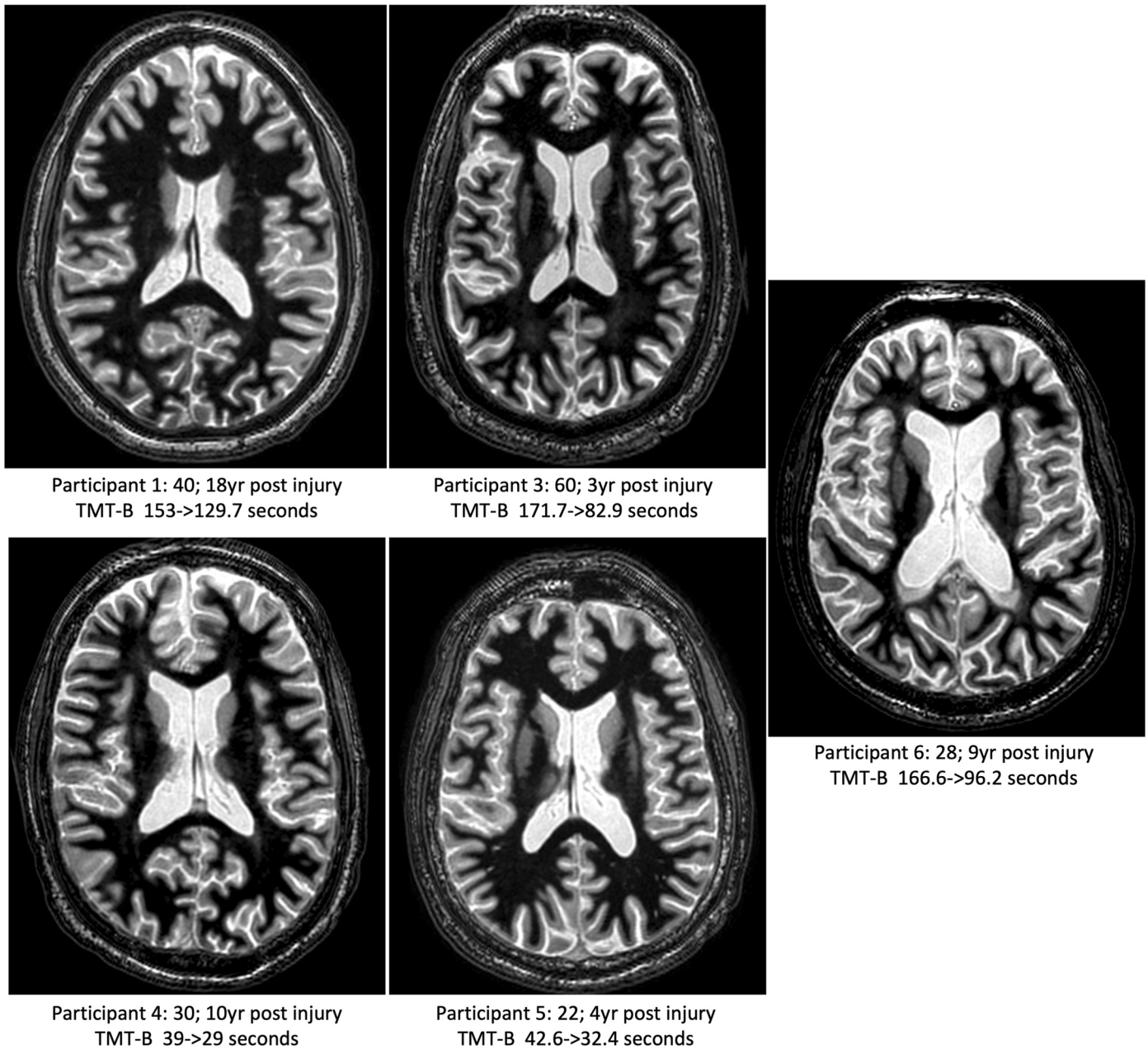
electrodes). As seen in each panel, postsurgical electrode placement is medial to planned location. As shown in Fig. 5, a relative symmetry of cortical response is nonetheless obtained suggesting that more medial fibers associated with this pattern activation did not appear in the DTI model due to the loss of local signal in the region of the hemorrhage.

Participant 6 (P6)



Extended Data Fig. 7 | Placement of DBS electrodes within the CL/DTTm target for P6. **A.** Active contact locations and fiber bundles for left hemisphere of P6 rendered within P6 space, CL nucleus (red), MD (green), VPL (purple) Cm (cyan). DBS activation of fibers (red), inactive fibers rendered in blue. **B.** Histograms of fiber activation for left sided CL, MD, VPL, and Cm. **C.** DBS

activation of fibers (red), inactive fibers rendered in blue. **D.** Active contact locations and fiber bundles for right hemisphere of P6 rendered within P6 space, CL nucleus (red), MD (green), VPL (purple) Cm (cyan). **E.** Histograms of fiber activation for right-sided CL, MD, VPL, and Cm. **F.** DBS activation of fibers (red), inactive fibers rendered in blue.



Extended Data Fig. 8 | Structural MRI imaging overview all 5 subjects. Figure shows representative horizontal MRI image from each participant along with demographic information and change in TMT-B performance from presurgical to treatment end timepoint.

Extended Data Table 1 | Trial-Making-Test and Cognitive Self-Report Measure Results

Participant	1	3	4	5	6	Mean
TMT--Raw Scores						
Part B						
Pre-surgery baseline	153.0	171.7	39.0	42.6	166.6	114.6
Treatment end	129.7	82.9	29.0	32.4	96.2	74.0
Percent change	-15.2	-51.7	-25.6	-23.9	-42.3	-31.8
Part A						
Pre-surgery baseline	62.0	85.9	22.1	18.7	61.6	50.1
Treatment end	41.5	45.9	16.5	14.7	44.7	32.7
Percent change	-33.1	-46.6	-25.3	-21.4	-27.4	-30.8
TMT--Demographically Adjusted T-Scores:						
Part B						
Pre-surgery baseline	22	33	62	62	22	40.2
Treatment end	22	50	71	71	35	49.8
Change over time	0	17	9	9	13	9.6
Part A						
Pre-surgery baseline	21	20	49	57	22	33.8
Treatment end	30	38	66	71	31	47.2
Change over time	9	18	17	14	9	13.4
QoL Attention						
Pre-surgery baseline	19	6	14	10	14	12.6
Treatment end	30	10	21	23	27	22.2
Percent change	58	67	50	130	93	79.5
QoL Executive Function						
Pre-surgery baseline	36	20	25	28	24	26.6
Treatment end	43	20	32	43	39	35.4
Percent change	19	0	28	54	63	32.7

Table shows pre- and post-trial results of TMT and related TBIQoL Attention and Executive function self-report measures for each participant.

Extended Data Table 2 | Localization of active contacts within synthetic atlas, means and variances

Patient ID	Left Lead Active Contact Coordinates			
	Active Contact	R/L Coordinate	A/P Coordinate	S/I Coordinate
P1	L4	-13.90	-4.32	9.62
	L3	-13.10	-5.85	7.00
P3	L4	-13.50	-3.90	8.80
	L3	-12.85	-5.10	6.00
P4	L4	-11.80	-5.20	6.80
	L3	-11.65	-7.10	4.10
	L2*	-11.30	-8.60	1.90
P5	L4	-13.05	-6.60	8.25
	L3	-12.45	-8.20	5.85
P6	L4	-11.10	-5.40	7.90
	L3	-10.70	-7.10	5.80
Top Active Contact: Mean		-12.67	-5.08	8.27
Top Active Contact: Standard Deviation		1.18	1.05	1.05
Bottom Active Contact: Mean		-12.15	-6.67	5.75
Bottom Active Contact: Standard Deviation		0.98	1.21	1.04
Patient ID	Right Lead Active Contact Coordinates			
	Active Contact	R/L Coordinate	A/P Coordinate	S/I Coordinate
P1	R4	8.60	-4.10	8.20
	R3	8.10	-5.10	5.40
P3	R4	7.40	-4.85	6.85
	R3	7.00	-6.10	4.40
P4	R4	7.40	-2.10	9.70
	R3	7.00	-3.60	7.50
	R2*	6.40	-5.10	4.70
P5	R4	8.60	-4.10	9.40
	R3	8.10	-5.70	7.05
P6	R4	8.60	-6.50	8.55
	R3	9.00	-8.50	6.35
	R2	9.40	-10.35	4.00
Top Active Contact: Mean		8.30	-4.89	8.25
Top Active Contact: Standard Deviation		0.60	1.13	1.06
Bottom Active Contact: Mean		7.84	-5.80	6.14
Bottom Active Contact: Standard Deviation		0.85	1.78	1.25

Note, for contact R4 position numbers grayed out to reflect shorted contact.

Reporting Summary

Nature Portfolio wishes to improve the reproducibility of the work that we publish. This form provides structure for consistency and transparency in reporting. For further information on Nature Portfolio policies, see our [Editorial Policies](#) and the [Editorial Policy Checklist](#).

Statistics

For all statistical analyses, confirm that the following items are present in the figure legend, table legend, main text, or Methods section.

n/a Confirmed

- The exact sample size (n) for each experimental group/condition, given as a discrete number and unit of measurement
- A statement on whether measurements were taken from distinct samples or whether the same sample was measured repeatedly
- The statistical test(s) used AND whether they are one- or two-sided
Only common tests should be described solely by name; describe more complex techniques in the Methods section.
- A description of all covariates tested
- A description of any assumptions or corrections, such as tests of normality and adjustment for multiple comparisons
- A full description of the statistical parameters including central tendency (e.g. means) or other basic estimates (e.g. regression coefficient) AND variation (e.g. standard deviation) or associated estimates of uncertainty (e.g. confidence intervals)
- For null hypothesis testing, the test statistic (e.g. F , t , r) with confidence intervals, effect sizes, degrees of freedom and P value noted
Give P values as exact values whenever suitable.
- For Bayesian analysis, information on the choice of priors and Markov chain Monte Carlo settings
- For hierarchical and complex designs, identification of the appropriate level for tests and full reporting of outcomes
- Estimates of effect sizes (e.g. Cohen's d , Pearson's r), indicating how they were calculated

Our web collection on [statistics for biologists](#) contains articles on many of the points above.

Software and code

Policy information about [availability of computer code](#)

Data collection

Data analysis

For manuscripts utilizing custom algorithms or software that are central to the research but not yet described in published literature, software must be made available to editors and reviewers. We strongly encourage code deposition in a community repository (e.g. GitHub). See the Nature Portfolio [guidelines for submitting code & software](#) for further information.

Data

Policy information about [availability of data](#)

All manuscripts must include a [data availability statement](#). This statement should provide the following information, where applicable:

- Accession codes, unique identifiers, or web links for publicly available datasets
- A description of any restrictions on data availability
- For clinical datasets or third party data, please ensure that the statement adheres to our [policy](#)

A minimum dataset extracted from the REDCAP database has been made available on Dryad: https://datadryad.org/stash/share/qj1U_HqZYVgzadpn9vxF2CE6hhvGEQYHjARTQ3zs6uU

Research involving human participants, their data, or biological material

Policy information about studies with [human participants or human data](#). See also policy information about [sex, gender \(identity/presentation\), and sexual orientation](#) and [race, ethnicity and racism](#).

Reporting on sex and gender	We sought to recruit participants representative of the general population of those with msTBI in terms of sex which is anticipated to yield a 2:1 Male:Female ratio. We enrolled 4 men and 2 women based on self-report. We did not collect disaggregated sex and gender information. Given the small N of the study and the reporting of sex only, we do not report any sex and gender-based analyses.
Reporting on race, ethnicity, or other socially relevant groupings	We enrolled 4 men (white) and 2 women (white).
Population characteristics	1. History of moderate to severe TBI based on estimated GCS score within first 48 hours of injury (acceptable GCS range = 3-12); 2. Age 22-60; 3. At least 24 months from date of onset; 4. Fluent in English and able to independently provide consent; 5. Rating of lower moderate disability to lower good recovery on the Glasgow Outcome Scale-Extended (GOSE) at time of enrollment (acceptable GOSE range 5-7); 7. Failure to return to pre-injury level of vocational or educational function.
Recruitment	Participant recruitment Participants were recruited through a variety of channels, including self-referral and provision of IRB-approved recruitment materials to academic research partners and consumer advocacy organizations serving patients with TBI. To accelerate enrollment, we also received IRB approval to subcontract with PatientWing (Philadelphia, PA), a digital media marketing firm specializing in clinical trial recruitment. PatientWing identified potential study candidates using key-word searches on several online platforms including Google and various social media channels. To ensure equal access to our trial, PatientWing also launched a print campaign during the heavy holiday travel season in several Greyhound bus stations throughout California, targeting individuals without access to the internet. Candidates initially underwent telephone screening, which included administration of the Glasgow Outcome Scale-Extended (GOS-E) Structured Interview to ensure that the candidate had not returned to pre-injury level of vocational or educational function (GOS-E rating no higher than 5). Through these efforts, 419 inquiries were received and 15 individuals were consented for further assessment to confirm eligibility. Of these, 9 candidates were excluded and 6 met all eligibility criteria and were randomized (See CONSORT Diagram). All recruited patients responded to advertised information about the study potentially biasing the sample recruited to those able to search for information or looking for clinical studies.
Ethics oversight	All sites designated to the single Stanford University IRB which maintained oversight of this study.

Note that full information on the approval of the study protocol must also be provided in the manuscript.

Field-specific reporting

Please select the one below that is the best fit for your research. If you are not sure, read the appropriate sections before making your selection.

Life sciences Behavioural & social sciences Ecological, evolutionary & environmental sciences

For a reference copy of the document with all sections, see [nature.com/documents/nr-reporting-summary-flat.pdf](https://www.nature.com/documents/nr-reporting-summary-flat.pdf)

Life sciences study design

All studies must disclose on these points even when the disclosure is negative.

Sample size	6 participants; FDA feasibility study under IDE; population size determined in conjunction with the FDA. 6 participants considered sufficient for establishing safety testing at the level of early feasibility trial.
Data exclusions	One secondary measure, Ruff 2&7 test, was excluded for participant P1 due to a test administration error detected by quality assurance procedures as reported in the manuscript.
Replication	Replication was tested by applying the same test batteries and measurement procedures across the study population. Replication was tested

Replication	in 5 sets of individual participant data obtained at pre-surgical and treatment end time points for all measures with the noted exception above of the secondary Ruff 2& 7 test which was excluded from this replication for one participant, P1, due to a test administration error on the first (pre-surgical) administration of the test.
Randomization	Participants were randomized into three cohorts that varied the time after implantation surgery prior to initial titration of stimulation and to conditions of a washout phase following treatment end phase. Procedures are described in the manuscript.
Blinding	Group membership was blinded to study investigators and unblinding of conditions occurred only after closure of the REDCAP database.

Reporting for specific materials, systems and methods

We require information from authors about some types of materials, experimental systems and methods used in many studies. Here, indicate whether each material, system or method listed is relevant to your study. If you are not sure if a list item applies to your research, read the appropriate section before selecting a response.

Materials & experimental systems

Methods

n/a	Involvement in the study
<input checked="" type="checkbox"/>	<input type="checkbox"/> Antibodies
<input checked="" type="checkbox"/>	<input type="checkbox"/> Eukaryotic cell lines
<input checked="" type="checkbox"/>	<input type="checkbox"/> Palaeontology and archaeology
<input checked="" type="checkbox"/>	<input type="checkbox"/> Animals and other organisms
<input type="checkbox"/>	<input checked="" type="checkbox"/> Clinical data
<input checked="" type="checkbox"/>	<input type="checkbox"/> Dual use research of concern
<input checked="" type="checkbox"/>	<input type="checkbox"/> Plants

n/a	Involvement in the study
<input checked="" type="checkbox"/>	<input type="checkbox"/> ChIP-seq
<input checked="" type="checkbox"/>	<input type="checkbox"/> Flow cytometry
<input type="checkbox"/>	<input checked="" type="checkbox"/> MRI-based neuroimaging

Clinical data

Policy information about [clinical studies](#)

All manuscripts should comply with the ICMJE [guidelines for publication of clinical research](#) and a completed [CONSORT checklist](#) must be included with all submissions.

Clinical trial registration

Study protocol

Data collection

Outcomes

Magnetic resonance imaging

Experimental design

Design type

Design specifications

Behavioral performance measures

Acquisition

Imaging type(s)

Field strength

Sequence & imaging parameters

acceleration: 2, scan time 11min.

Area of acquisition

Whole brain

Diffusion MRI

 Used Not used

Parameters 2D diffusion-weighted single-shot spin-echo echo planar imaging (EPI) sequence, axial orientation, TE 74ms, TR 8000ms, RBW

Preprocessing

Preprocessing software

Whole-brain WMn volumes were processed with the THOMAS thalamic segmentation tool with no preprocessing. The THOMAS algorithm applied to WMn images has been validated against manual segmentation³⁵. Using version v0 of this tool (<https://github.com/sujason/thomas>), we segmented and extracted the volumes of 12 lateralized structures in each hemisphere of the brain

Normalization

Each individual patient data used in subsequent pipeline; in addition a synthetic atlas used for group comparisons.

Normalization template

For the group analyses a synthetic atlas was developed to organize all participant electrode placements within a single common brain space (see Methods). The atlas was created by warping all individual image volumes to a common template using Advanced Normalization Tools software (ANTs, <http://stnava.github.io/ANTs/>), followed by averaging the warped volumes together. More specifically, white matter-nulled MRI image volumes from each of the five participants were combined using nonlinear registration to produce a template or synthetic atlas volume, representative of all participants

Noise and artifact removal

WMnMPRAGE and DTI image volumes were visually inspected to ensure that scans were of sufficient quality for analysis and were not corrupted by motion artifact.

Volume censoring

N/A

Statistical modeling & inference

Model type and settings

N/A

Effect(s) tested

N/A

Specify type of analysis: Whole brain ROI-based Both

Statistic type for inference

Specify voxel-wise or cluster-wise and report all relevant parameters for cluster-wise methods.

(See [Eklund et al. 2016](#))

Correction

Describe the type of correction and how it is obtained for multiple comparisons (e.g. FWE, FDR, permutation or Monte Carlo).

Models & analysis

n/a | Involved in the study

 Functional and/or effective connectivity Graph analysis Multivariate modeling or predictive analysis